Temozolomide treatment alters mismatch repair and boosts mutational burden in tumor and blood of colorectal cancer patients

Temozolomide treatment alters mismatch repair and boosts mutational burden in tumor and blood of colorectal cancer patients

Giovanni Crisafulli[1,2,10], Andrea Sartore-Bianchi[3,4,10], Luca Lazzari[6,10], Filippo Pietrantonio[5], Alessio Amatu[3], Marco Macagno[2], Ludovic Barault[1,2], Andrea Cassingena[3], Alice Bartolini[2], Paolo Luraghi[6], Gianluca Mauri[4,6], Paolo Battuello[1], Nicola Personeni[7,8], Maria Giulia Zampino[9], Valeria Pessei[2], Pietro Paolo Vitiello[1,2], Federica Tosi[3], Laura Idotta[3], Federica Morano[5], Emanuele Valtorta[3], Emanuela Bonoldi[3], Giovanni Germano[1,2], Federica Di Nicolantonio[1,2,11], Silvia Marsoni[6,11], Salvatore Siena[3,4,11], Alberto Bardelli[1,2,11]*

[1]Department of Oncology, University of Torino, Candiolo, Italy.
[2]Candiolo Cancer Institute, FPO - IRCCS, Candiolo, Italy.
[3]Niguarda Cancer Center, Grande Ospedale Metropolitano Niguarda, Milan, Italy.
[4]Department of Oncology and Hemato-Oncology, Università degli Studi di Milano, Milan, Italy.
[5]Department of Medical Oncology, Fondazione IRCCS Istituto Nazionale dei Tumori, Milan, Italy.
[6]The FIRC Institute of Molecular Oncology, Milan, Italy.
[7]Department of Biomedical Sciences, Humanitas University, Via Rita Levi Montalcini 4, 20090 Pieve Emanuele, Milan, Italy.
[8]Medical Oncology and Hematology Unit, Humanitas Cancer Center, IRCCS Humanitas Research Hospital, Via Manzoni 56, 20089 Rozzano, Milan, Italy.
[9] Division of Gastrointestinal Medical Oncology and Neuroendocrine Tumors European Institute of Oncology, IRCCS, Milan, Italy

[10]These authors contributed equally
[11]Co-senior authors
*Corresponding author:

Alberto Bardelli

Email: alberto.bardelli@unito.it

KEYWORDS

Colorectal Cancer, Mismatch Repair, Temozolomide, Mutational Signature, MSH6

ADDITIONAL INFORMATION

Financial support:

The research leading to these results has received funding from FONDAZIONE AIRC under 5 per Mille 2018 - ID. 21091 program – P.I. Bardelli Alberto (A.B.) and Group Leader Federica Di Nicolantonio (F.D.N.), Silvia Marsoni (S.M.) and Salvatore Siena (S.S.); AIRC under IG 2018 - ID. 21923 project – P.I. Bardelli Alberto (A.B.); AIRC under IG 2018 - ID. 21407 project – P.I. Di Nicolantonio Federica (F.D.N.); International Accelerator Award, ACRCelerate, jointly funded by Cancer Research UK (A26825 and A28223), FC AECC (GEACC18004TAB) and AIRC (22795); BiLiGeCT - Progetto PON ARS01_00492. Fondazione Oncologia Niguarda provided financial support for temozolomide supply and logistics. MSD Italy provided drug and financial support.

Corresponding author

Alberto Bardelli
Email: alberto.bardelli@unito.it
Phone and fax number: (+39) 011 993 3235
Mailing address: University of Turin, Dept. Oncology, Candiolo Cancer Institute, FPO-IRCCS Str.Prov.le 142, km 3.95 ZIP: 10060, Candiolo (To) – Italy

Conflict of interest disclosure statement

A.Bardelli served in a consulting/advisory role for Illumina and Inivata. A.Bardelli and G.G. are cofounders and shareholders of NeoPhore. A.Bardelli is a member of the NeoPhore scientific advisory board. N.P. received consulting fees from Amgen, Merck Serono, Servier; lectures fees from AbbVie, Gilead, Lilly, Sanofi; travel support from Amgen, ArQule; and institutional research funding from Basilea, Merck Serono, Servier. A.S.B. is a member of advisory boards for Amgen, Bayer, Sanofi and Servier. S.S. is an advisory board member for AstraZeneca, Bayer, BMS, CheckmAb, Daiichi-Sankyo, Menarini, Merck, and Seattle Genetics. F.P. received honoraria from Merck-Serono, Amgen, Sanofi, Lilly, Servier, Bayer, Astrazeneca and research Grants from BMS, AstraZeneca. The other authors declare no competing financial interests.

Abstract

The majority of metastatic colorectal cancers (mCRC) are mismatch repair (MMR) proficient and unresponsive to immunotherapy, while MMR deficient (MMRd) tumors often respond to immune checkpoint blockade (ICB). We previously reported that treatment of CRC preclinical models with temozolomide (TMZ) leads to MMR deficiency, increased tumor mutational burden (TMB) and sensitization to immunotherapy. To clinically translate these findings, we designed the ARETHUSA clinical trial whereby O6-Methylguanine-DNA-methyltransferase (MGMT) deficient MMR proficient mCRC patients received priming therapy with TMZ. Analysis of tissue biopsies and circulating tumor DNA (ctDNA) obtained after TMZ treatment, revealed the emergence of a distinct mutational signature and increased TMB. Multiple alterations in the nucleotide context favored by the TMZ signature emerged in MMR genes in all post TMZ samples, and the p.T1219I *MSH6* variant was detected in ctDNA and tissue of 94% (16/17) of the cases. A subset of the patients whose tumors displayed the *MSH6* mutation, the TMZ mutational signature and increased TMB, achieved disease stabilization upon pembrolizumab treatment.

STATEMENT OF SIGNIFICANCE

Mismatch-repair (MMR) proficient mCRCs are unresponsive to immunotherapy. We provide *proof-of-concept* that inactivation of the MMR genes can be achieved pharmacologically with temozolomide and can be molecularly monitored in tissue and blood of mCRC patients. This strategy deserves further evaluation in mCRC patients whose tumors have run short of SOC-treatments.

INTRODUCTION

Colorectal cancer (CRC) is one of the most common and lethal cancers, representing around 10% of new cancer diagnoses and 9% of cancer-related deaths (1, 2). While the 5-year relative overall survival (OS) ranges between 68-90% in localized disease (stage I-III), in stage IV metastatic CRC (mCRC) it is still dismal, dropping to 11-14%(1, 2).

Cytotoxic combinations represent the main therapeutic options for most mCRC patients (3, 4). Despite recent progresses exploiting targeted therapies such as combination of BRAF and EGFR inhibitors for *BRAF*^{V600E} mutant tumors, or HER2-blockade in HER2-positive ones, treatment developments have been incremental rather than transformative (5-9).

The Mismatch Repair (MMR) system, which detects and corrects base mispairs, insertions and deletions (INDELs) that occur during DNA synthesis, is deregulated in approximately 15% stage I-III CRC and 4-5% mCRC (10, 11). Based on the MMR proficiency status, CRCs are classified into two molecularly distinct subgroups defined as mismatch repair proficient (MMRp) or deficient (MMRd) (12, 13). MMRp tumors include those that are usually microsatellite stable (MSS) or tumors with intact MMR proteins, accounting for around 95% mCRCs (14). MMRd tumors usually present microsatellite instability (MSI) as a consequence of genetic or epigenetic alterations leading to inactivation of MMR genes, such as *MLH1*, *MSH2*, *MSH6* and *PMS2* (15). As a result of a defective MMR machinery, MMRd tumor cells display a high number of genomic alterations leading to the production of non-self-peptides, which should be recognized by the immune system (16, 17). This hypothesis is consistent with the observation that MSI/MMRd CRCs are counter selected during progression towards metastatic disease and display an overall better prognosis with respect to the MSS/MMRp counterpart (18). Immune therapy based on anti-programmed death-1 (PD-1) agents is highly effective in MSI/MMRd mCRC patients. In first line, the anti PD-1 agent pembrolizumab led to superior progression-free survival (PFS) compared to chemotherapy for MSI/MMRd mCRC (19). In the same setting, a single-arm phase II trial found that also the combination of another anti PD-1, nivolumab, plus low-dose of the anti-cytotoxic T-lymphocyte antigen 4 (CTLA4)

ipilimumab demonstrated an extremely high rate of durable clinical benefit (20). The latter combination is now being tested in a confirmatory randomized phase III trial versus nivolumab alone or physician's choice chemotherapy (Checkmate 8HW trial NCT04008030). In patients with chemo-refractory disease, results from phase II trials with pembrolizumab (21) or the combination of nivolumab and ipilimumab (22) had also shown promising efficacy in terms of response rate (RR) and PFS providing the grounds for escalation to first-line. As a whole, these results are radically transforming treatment guidelines and impact on real-world MSI/MMRd mCRC patients (23)

A rare subset of MSS mCRCs harboring mutations in the exonuclease domain of DNA polymerase epsilon (*POLE*) gene display an ultra-mutated phenotype with significantly higher tumor mutational burden (TMB) than MSI/MMRd CRCs. POLE mutant MSS tumors are characterized by a high number of single nucleotide variants (SNVs) and have also been found exquisitely sensitive to immune checkpoint blockade (ICB) (14, 24). Interestingly, both MSI carrying elevated levels of indels/frameshifts and POLE mutant CRC (characterized by elevated SNVs and much less indels/frameshifts) benefit from immunotherapy. This indicates that both classes of genetic alterations can trigger an immune response.

While ICB dramatically impacted the prognosis of MSI/MMRd and MSS POLE mutant mCRC patients, MSS/MMRp mCRCs are intrinsically resistant to anti-PD-1-based regimens (25). Indeed, MSS/MMRp mCRCs are characterized by low TMB, an immune suppressive tumor microenvironment with low level of tumor infiltrating lymphocytes, and a reduced expression of checkpoint proteins (17). Thus, MSS/MMRp mCRCs are usually defined as "*cold*" as opposed to the "*immunologically hot*" MSI/MMRd counterpart (17). One of the current greatest challenges for translational research in mCRC is to understand how to switch immunologically "*cold*" into "*hot*" tumors.

Different combinations of checkpoint inhibitors with cytotoxic, anti-vascular endothelial growth factor (anti-VEGF), anti-EGFR agents or tyrosine kinase inhibitors have been tested in clinical trials in MSS/MMRp mCRCs, but overall results remain disappointingly inconclusive (14, 26-30).

The alkylating agent temozolomide (TMZ) is a treatment option in several solid tumors such as glioma, glioblastoma, neuroendocrine tumors, melanoma and sarcomas (31-37). Resistance to TMZ in *O(6)-methylguanine-DNA methyltransferase (MGMT)* methylated glioblastomas is associated with the onset of inactivating mutations in MMR genes, such as *MSH6* (38-41). Recurrent tumors are more frequently hypermutated, which may potentially sensitize glioblastomas to ICB (42, 43). This observation led to a currently ongoing phase II trial assessing the effectiveness of ICB in recurrent hypermutated glioma and glioblastoma (NCT04145115 and NCT02658279).

Using a syngeneic CRC mouse model, our group previously demonstrated that TMZ treatment led to the emergence of MMRd cells among an otherwise MMRp cell population (44). Interestingly, these cells were more immunogenic and triggered immune surveillance in mice (44). Additionally, analysis of tumor biopsies from mCRC patients relapsing after TMZ-based therapeutic regimens revealed MMR mutations as a potential resistance mechanism in two out of five cases (44). Finally, our data suggested that MMR inactivation in mouse and human CRCs could lead to increased TMB and predicted neoantigens (44). These data led to the design of the ongoing ARETHUSA (NCT03519412), a *proof-of-concept* two-step clinical trial. During the first step – the *priming* phase - TMZ treatment is used both with therapeutic intent and to trigger a hypermutant status in MGMT-hypermethylated MSS mCRC patients. In the second step - the *immunotherapy* phase - the anti-PD-1 agent pembrolizumab is deployed as monotherapy in those patients who develops a TMB $\geq$ 20 mut/Mb upon progression after TMZ treatment.

Here we present the analyses of tissue biopsies and circulating tumor DNA (ctDNA) obtained from an initial cohort of 21 ARETHUSA patients before and after the *priming* phase. We provide clinical *proof-of-concept* that targeting DNA repair processes can impact the mutational evolution of MSS/MMRp tumors and be potentially exploited as a non-canonical strategy to turn immunologically "*cold*" into "*hot*" tumors.

RESULTS

Clinical flow and logistics of the ARETHUSA trial

We selected *RAS* mutated mCRC patients who had progressive disease (PD) on or after prior systemic treatment including fluoropyrimidines, oxaliplatin, irinotecan, regorafenib, or trifluridine/tipiracil. All patients were screened for MMR and/or MSI status on archival formalin-fixed paraffin-embedded (FFPE) tumor tissues.

The status of the *MGMT* gene and protein is evaluated during the *screening* phase before enrolling the patient in the *priming* phase. To enter this phase, eligible patients must have tumors: i) with no or low expression of MGMT protein as defined by a negative IHC staining, and ii) with hypermethylation at the *MGMT* gene promoter level as defined by a positive MethylBEAming analysis. These are mandatory criteria for the molecular screening of patients before enrollment. We previously demonstrated that *MGMT* methylated mCRC are more likely to benefit from TMZ than those lacking *MGMT* methylation (45-49). Accordingly, TMZ priming was restricted to patients with MGMT defective tumors assessed by both protein expression and promoter methylation since this two-layer selection has been identified as the most effective by a large pooled cohort in this setting (49). Patients were also biopsied pre (non-mandatory) and post (mandatory) TMZ treatment, to determine the post-TMZ TMB and whenever possible, any changes in TMB over time (Figure 1). A post-TMZ threshold of 20 mutations/Mb (i.e. double that required for the Standard of Care (SOC) use of the anti-PD1 antibody pembrolizumab) (15, 50) was required to access the *immunotherapy* phase delivering pembrolizumab every three weeks until PD or unacceptable toxicity (Figure 1). The ARETHUSA clinical trial is currently ongoing and recruiting mCRC patients (NCT03519412), while the translational analyses of an initial cohort of 21 patients enrolled in the trial are presented here.

Clinical efficacy of TMZ in the priming phase of the ARETHUSA trial

From February 2019 to December 2021 (data lock for the present study), 473 MSS/MMRp *RAS* mutant mCRC patients were enrolled in the study, 442 patients were screened for MGMT status and 33 of 69 *MGMT* methylated patients received priming treatment with TMZ. Twenty-seven patients were treated with TMZ until PD,

while treatment of 6 patients was currently ongoing at the time of data lock. We included in ARETHUSA three additional patients who had PD on TMZ-based regimens as part of other trials (51, 52) or on TMZ off-label treatment (Supplementary Figure S1). Of the 30 patients treated in the priming phase until PD, TMZ was administered for a median of 3.0 months of treatment [range 0.6-7.5] (Figure 2). TMZ priming achieved a disease control rate (DCR) of 57% (17/30, 57%; 95%CI 39-74%). Unsurprisingly, in a heavily pre-treated *RAS* mutant patient population such as in ARETHUSA [median prior regimen N=3 (range 1-60); 63 % (19/30) of patients with previous $\geq$3 therapeutic line], DCR consisted of disease stabilization (SD) as RECIST1.1 best response, with a median PFS of 4.2 months (range 2.7-7.5; Figure 2). However, tumor growth stabilization lasting $\geq$ 4 months (corresponding to at least 5 cycles of TMZ) was achieved in 10 of 17 patients (10/17, 59%; 95% CI 35-82%). The median PFS in patients experiencing PD as best response was 2.0 months (range 0.6-2.4; Figure 2). A post-TMZ biopsy was performed in 21 patients at PD (Figure 2 and supplementary S1 and Table S1). Biopsy at PD was not performed in 9 cases due to the deteriorating patients' clinical conditions (Figure 2).

TMZ was tolerated as expected in this setting, without drug-related serious adverse events (SAEs) except for hematological (neutropenia/thrombocytopenia; n=1) and gastrointestinal (n=1) toxicities, consistently with previous studies (45, 47). Particularly, neither death nor life-threatening serious adverse events (SAEs) have been reported. In summary, TMZ priming can be safely delivered as a third/fourth line treatment in *MGMT* hypermethylated, *RAS* mutated mCRC patients and tissue biopsies can be obtained at PD in most patients.

Identification of the TMZ signature in CRC cells treated with TMZ

Somatic mutations are caused by distinct mutational processes, generating characteristic mutational signatures which can be detected in the genome of cancer cells (53-56). The analysis of mutational signatures using the "fitting" method involves a sequence of mathematical steps designed to identify the best-known signatures (or combination of thereof) that can explain the observed mutational profile in an individual sample (57). Many of these signatures have been associated with a defined etiology, including exposure to a specific treatment, known

carcinogens, defective or error-prone DNA repair proteins (53, 54, 58). Notably, previous works have shown that mutational signature analyses can readily identify the effect of alkylating agents such as TMZ (53, 54, 58). In particular, mutational signature 11 (single base substitutions 11 or SBS11) was found in malignant melanoma or glioblastoma patients and was previously reported in experimental studies with alkylating agents (53, 54, 58). We reasoned that mutational signature assessment in tissue samples collected at the end of the priming phase could help to mechanistically determine the molecular impact and the functional implications of TMZ treatment and predict the efficacy of subsequent immunotherapies in ARETHUSA patients.

To assess the specificity of signature profile identification, we examined whole exome sequencing (WES) data from a panel of 12 cell lines, including MSS, MSI and *POLE*-mutated models. As shown in Supplementary Figure S2A, Signature 1 (age related) was readily identified in all cell lines, while signatures 6/15/26 (associated to MMR deficiency) and signature 10 (related to *POLE* mutations) were detected in MMRd/MSI and *POLE*-mutated cell models, respectively (Figure S2A). Next, as positive control to demonstrate the proper identification of TMZ signature in the CRC genome, we treated two *MGMT* methylated CRC cell models (SKCO1 and SW620) with TMZ, as previously reported (44). For both parental and TMZ treated cells genetic analyses have been performed to systematically detect mutational signatures. As expected, the alkylating agent related signature 11 was evident only in CRC cells treated with TMZ, confirming the specificity of the approach (Supplementary Figure S2B).

Detection of the TMZ signature in tumor biopsies after treatment with TMZ

Upon validation in cell models, the approach was then employed to identify mutational signatures using WES data of post-TMZ tumor samples collected from all 21 biopsied patients (Supplementary Table S1 and Figure S1). Tumor biopsies obtained at TMZ progression, were analyzed to evaluate TMB and establish the eligibility to pembrolizumab treatment (Figure 1). TMB analysis was also performed on samples from 5 patients with an available pre-TMZ tissue biopsy (Figure 1). Mutation calling was initially performed using a threshold variant allelic frequency (VAF) value ≥ 10% to select molecular alterations occurring in a predominantly

clonal fashion (as reported in (15)). Using this approach, two patients (AR02007 and AR01052) scored positive for the alkylating agent related signature 11 (Figure 3A). In these two cases 78% and 77% of the mutations could be attributed to TMZ treatment, respectively (Figure 3A).

We reasoned that, as for other anticancer therapies, molecular changes triggered by TMZ treatment were likely to occur at subclonal levels and in an heterogenous manner. To evaluate this possibility, we performed mutational signature analysis considering also somatic variants with variant allele frequency (VAF) < 10% (subclonal analysis). This was feasible considering that we sequenced high quality DNA obtained from fresh tissues and used a high-depth sequencing approach (median depth 376X with PhredScore ≧ 30 and coverage ≥ 96.82% at 100X depth; Supplementary Table S1) which gathered a median of 124 million reads per sample (Supplementary Table S1).

Using clonal and subclonal combined TMZ mutational profiling, we found that CRC samples from ARETHUSA patients could be classified in two main categories, that we named Subtype A and B: Subtype A (N=4) encompasses tumor samples scoring negative for signature 11, and includes patients who received a few TMZ cycles (Figure 3AB and Supplementary Table S2). Instead, Subtype B (N=17) features tissue samples collected from patients who received longer TMZ treatment and in which signature 11 can be identified (Figure 3AB and Supplementary Table S2). Notably, according to the clonality score of the variants used to detect signature 11, the subtype B could be further subdivided in two sub-classes (Figure 3AB). Subtype B1, including all those tumor samples in which signature 11 is detected at subclonal level (N=15, Figure 3AB), and subtype B2 in which the presence of signature 11 is defined at clonal level (N=2, Figure 3AB).

While in subtype B1 only a fraction of the cells evaluated in the biopsy are affected by the TMZ treatment and acquire signature 11, in subtype B2 a larger fraction of the tumor cells displays the characteristic molecular imprint of the TMZ treatment (Figure 3AB). In five cases (AR02071, AR01032, AR01014, AR01069 and AR02064), the number of mutations was not sufficient to properly perform mutational analysis of clonal variants, and these samples were excluded from the analysis (cosine similarity lower than 0.9, see Figure S2CD and method section for details).

To exclude that patient stratification in subtypes A, B1 and B2 could be affected by the reference signatures that were used for the mutational analysis fitting, we performed clonal and subclonal scrutiny using three reference signature databases available in COSMIC (v 2.0, v 3.0 and v 3.2) and two distinct bioinformatic tools (see methods for details). These analyses led to comparable results (Figure 3AB and Supplementary Figure S3).

To evaluate how patient stratification was affected by the heterogeneity of the tumor biopsy, we checked the performance of the clonal/subclonal analysis comparing the reconstructed mutational profile (after fitting) with the original mutational profile of the sample using the cosine similarity as parameter (59, 60). The cosine similarity parameter quantifies two-vector similarities and spans from 1 (identical) to 0 (distinct). A high cosine similarity value (closer to 1) indicates suitable reconstruction of the processes determining mutation accumulation (59, 60). We found that cosine similarity was always higher than 0.90 and 0.95 in the clonal and subclonal analyses, respectively (Supplementary Figure S2CD). In summary, this observation supports the validity of the results obtained in the subclonal analysis, suggesting that it can confidently capture the relative contribution of each mutational signature (including the TMZ effect) and classify tumor samples based on the etiological origin of their mutations (Supplementary Figure S2CD).

Assessment of Tumor Mutational Burden in tissue biopsies after TMZ priming

TMB was calculated on high-depth WES of tumor tissue biopsies using peripheral blood mononuclear cells (PBMCs) as normal matched sample (Supplementary Table S1). We applied the same workflow used for the mutational signature analyses initially considering mutations with VAF ≥ 10%. Based on this cut off, patients AR02007 and AR01052 displayed 49 mut/Mb and 27 mut/MB respectively (Figure 3C); while all other cases displayed less than 10 mut/Mb (Figure 3C), a value commonly found in MSS CRCs (15). Interestingly, only the two patients with TMB ≥ 20 mut/MB (AR02007 and AR01052) also displayed a high clonal score for signature 11 (Figure 3A), while the remaining patients had low clonal TMB (< 10 mut/MB) and low Signature 11 score in post TMZ biopsies (Figure 3AC).

The availability of high depth NGS data (median depth 376X with PhredScore ≧ 30 and coverage ≥ 96.82% at 100X depth; Supplementary Table S1) allowed TMB assessment also at subclonal level (considering mutations with VAF < 10%). Samples from subtype A mCRC had an average subclonal TMB post-TMZ of 24 mut/Mb, while samples from subtype B had a higher average subclonal TMB post-TMZ of 152 mut/Mb (p.value < 0.0007, Figure 3C).

We also evaluated the SNVs and INDELs contribution to TMB value (Figure 3D). Notably, a prominent impact of TMZ on the tumors (from left to right in the Figure 3) was paralleled by an increase of SNVs, while the absolute number of INDELs remained similar in all tumors. This is in line with previous reports from our group and others (44, 53, 54).

Next, we studied whether and to what extent the number of TMZ cycles impacted the molecular profiles of post-TMZ biopsies. We noted that patients with subtype B mCRC and higher subclonal TMB had disease control (SD) with longer TMZ treatment than patients with subtype A mCRC, who experienced PD as best response without benefiting from TMZ thus receiving lower drug exposure (Figure 3CDE and Supplementary Table S2). Notably, a linear positive correlation between the number of mutations/megabase induced by TMZ Signature and cycles of TMZ treatment in patients was observed (Spearman rank correlation, R=0.7847, p.value 2.535e-5, Pearson R=0.6887, p.value 0.00055, inset of Figure 3C). This strongly suggests that molecular differences occurring in subtype B1/B2 could be attributed to the level of exposure to TMZ.

While a post-TMZ biopsy was mandatory for all ARETHUSA patients, an exploratory pre-TMZ biopsy was also performed in 5/21 patients (4 subtype B, 1 subtype A). These valuable samples allowed us to comparatively study the impact of TMZ on mutational signatures and TMB (Figure 4ABC). In these cases, comparison between matched pre and post TMZ treatment biopsies confirmed that SBS11 was absent in all samples obtained before the TMZ treatment in both patients with subtype A (Figure 4A) and subtype B1 (Figure 4B). These analyses further corroborated the

emergence of signature 11 post-TMZ in patients with subtype B1 (Figure 4B) and revealed that the increase of TMB was the highest in subtype B1 tumors (Figure 4C).

Assessment of Tumor Mutational Burden in blood before and after TMZ priming

Considering that tissue biopsies often represent only a spatial-temporal snapshot of the tumor genomic heterogeneity and that we detected molecular heterogeneity post-TMZ (subtypes A, B1 and B2), we also studied ctDNA, as this approach may more comprehensively capture the whole molecular profile of metastatic tumor (61, 62) and more easily integrate into the therapeutic path of patients than tissue biopsy. Conveniently, we had collected longitudinal blood samples including pre- and post-TMZ treatment for most patients (Figure 1). Blood tumor mutational burden (bTMB) was measured in plasma samples before and after TMZ treatment (Figure 1), using a validated assay for tissue/blood correlative analyses (63).

Collectively, bTMB values were comparable to those of subclonal TMB calculated by WES on tissue biopsies (Figure 3C and 4E) except for patients with lesions localized mainly in lung and/or peritoneum. In fact, differently from cases carrying predominantly liver lesions, in these patients (AR02011, AR01015 and AR01034) the maximum VAF detected in both pre- and post-TMZ blood samples was below 10% thus affecting bTMB (Supplementary Figure S5A and Supplementary Table S2). This is likely related to the impact of metastatic sites on ctDNA release capacity and detection, as recently reported (64). Interestingly, the two subtype B2 patients (AR02007 and AR01052, subtype B2 with clonal TMZ signature, Figure 3C) showed a bTMB value of 2276 and 196 mut/Mb, respectively (AR02007 and AR01052, subtype B2, Figure 4E).

Median bTMB value evaluated in basal plasma samples was 18.18 mut/Mb (Figure 4D). Comparison of bTMB in matched pre-post TMZ plasma samples allowed to conclude that in most patients high TMB values assessed in tissue were indeed induced by TMZ and that the ARETHUSA priming phase significantly increases bTMB (p=value 0.002443, Wilcoxon rank sum test, Figure 4DE).

Mutations in MMR genes in post TMZ treatment biopsies

We and others have shown that secondary resistance to anti-cancer therapies is associated with changes in the tumor mutational profiles, including emergence of mutations in key effectors of the pathway targeted by the anti-cancer drug (65, 66). Current knowledge on the resistance mechanisms to TMZ have been obtained studying glioma and glioblastoma (39), we were the first to report how secondary resistance to TMZ in CRC preclinical models, selects tumor cells carrying alterations in other genes involved in DNA MMR system, such as *MHL1* or *MSH6* (44). Those findings laid the preclinical rationale of the ARETHUSA design that is aimed at therapeutically exploiting the mutations induced by TMZ treatment. To this end, we used an integrated bioinformatic pipeline to assess SNVs, INDELs and gene copy-number alterations starting from WES data (67, 68). By comparing somatic alterations emerged in tissue samples post-TMZ, we identified a list of recurrently mutated genes. Interestingly, *MSH6* gene mutations recur upon treatment in multiple patients (8/17, 47% subtype B tumors). In particular, three *MSH6* mutations (p.T1219I, p.G557D and p.G1139S) were present in six ARETHUSA subtype B tissue but not in subtype A samples (Table 1). Functionally, these mutations have been found to decrease the efficiency of MMR machinery, as determined by *in-vitro* assays (69).

Recurrent MSH6 mutations in mCRC treated with TMZ

Plasma samples collected at pre- and post-TMZ time-points were analyzed to evaluate the genetic profile of MMR genes. Mutational profiles of ctDNA revealed again two main categories of patients, confirming the previous stratification based on subclonal signature analysis. The *MSH6* gene alterations were not detected in plasma/tissue samples of subtype A cases, but, strikingly, they were found in 17/17 (100%) of subtype B cases, with high prevalence of the *MSH6* p.T1219I variant (16/17, 94%). Importantly, it was never detected in the 5 tissue biopsies and all 20 plasma pre-TMZ samples available for the analysis (Table 1). Overall, these results indicate that in CRC the p.T1219I *MSH6* mutation emerges at very high frequency (94%) as a molecular response marker to extended exposure to TMZ. Given that the p.T1219I variant was never identified in subtype A cases (who also received TMZ), the occurrence of this variant does not simply reflect exposure to TMZ but it is also indicative of both molecular (TMB increase) and clinical (tumor response/stabilization) effects of TMZ treatment. Furthermore, the *MSH6* variant was

exclusively detected in patients positive for signature 11 (subclonal score > 0, subtype B tumors, Table 1).

Based on these findings, we formulated the hypothesis that the recurrent *MSH6* mutation was related to the TMZ mutational signature. To test this possibility, we checked whether the genomic region encoding the p.T1219I variant lies in the nucleotide context favored by signature 11 and indeed found that this was the case (Figure 5A). To exclude that the *MSH6* gene was enriched in nucleotide contexts favored by the emergence of mutational signature 11 (triplets mutated with high probability), we compared the sequence context of the *APC* gene (which served as control) and other MMR genes (Supplementary Figure S5A). The analysis revealed the absence of biases towards the *MSH6* sequence as compared to other MMR genes (Supplementary Figure S5A). Next, we reanalyzed tissue and ctDNA mutational profiles for additional variants and found that *MSH6* mutations could be detected in both tissue and matched ctDNA only when obtained after TMZ. Notably, virtually all (100%) of these SNVs were always causally linked to signature 11 (Table 1 and Figure 5AB).

TMZ-Signature and TMB change as a function of heterogeneity in CRC treated with TMZ

Metastases are highly heterogeneous, and the impact of heterogeneity on the pharmacodynamic response to TMZ priming in CRC patients is unknown. With the aim of inferring how a subset of TMZ resistant CRC cells impacted the TMB value and Mutational Signature 11 of the overall population, we exploited two TMZ sensitive (TMZ-S) CRC cell lines (SKCO1 and SW620) and their TMZ resistant (TMZ-R) derivatives that were generated by long-term drug exposure. We performed a new high-depth WES of DNA pools of both TMZ-S and TMZ-R cells composed of different fractions including: 100% TMZ-R; 50% TMZ-S, 50% TMZ-R; 75% TMZ-S, 25% TMZ-R; 87.5% TMZ-S, 12.5% TMZ-R; 93.75% TMZ-S, 6.25% TMZ-R; and 100% TMZ-S. In parallel, the same populations were created *in-silico* (see methods for detail) using different ratios of sequencing reads from WES data for both TMZ-S and TMZ-R cells. The correlation between TMB obtained by cell-based and *in-silico* mixtures analyses was 0.9968 (Pearson's product-moment correlation with p-value = 2.34e-12, Supplementary Figure S5A), confirming the robustness of this approach.

We then studied the effect of population heterogeneity on TMB increase and TMZ-signature detection in the SKCO1 TMZ-S cell line and its TMZ-R derivative. The analysis revealed that at least 30% TMZ-R cells are required to reach the TMB cut-off of 20 Mut/Mb using the clonal analysis, while as few as 2% TMZ-R cells were sufficient using the subclonal analysis (Supplementary Figure S5B). To be able to detect the TMZ-Signature, more than 25% of mutational signature 11 positive cells were required using the clonal analysis, while 6.25% cells were necessary to reach the sub-clonal threshold (Supplementary Figure S5CD). In conclusion, based on these results, when a clonal effect was detected, we expected that a 25-30% fraction of tumor cells displayed the TMZ scar; while in case of subclonal effect, we expected a fraction between 2-6% and 25-30% to display the TMZ scar.

Finally, we analyzed the impact of heterogeneity in the cell populations that acquired TMZ-resistance through the co-presence of two different mechanisms: the re-expression of MGMT and the acquisition of MMR gene mutations with increase of TMB and switching from MMRp to MMRd phenotype in the SW620 cell line. In this case, when only clonal mutations were considered, there was a modest increase of TMB that did not reach the 20 mut/MB cut-off (orange line in the Supplementary Figure S5E). When considering subclonal mutations, more than 50% of TMZ-R cells were required to overcome the 20 mut/MB cut-off (Supplementary Figure S5E). Due to the low number of acquired mutations, TMZ mutational signature 11 could not be retrieved when we applied a VAF $\geq$ 10% threshold (clonal mutations), For the same reasons, more than 25% of TMZ-R cells were required to detect the TMZ signature using subclonal alterations (Supplementary Figure S5F). Collectively, we showed how the mutational signature 11 and TMB change as function of heterogeneity of the population.

The previous preclinical results showed that the intratumor heterogeneity (ITH) plays a relevant role in the tissue analysis (TMB and genetic signatures), so we proposed that the differences between tissue tumor subtype B2 and B1 after TMZ treatment relies mainly on the fractional abundance of cells showing the TMZ genetic impact (Figure 6A). Next, we addressed the impact of ITH by analyzing three different

regions (corings) from the same liver lesion biopsy collected from patient AR02005 at progression of TMZ treatment (Figure 6B). Interestingly, the three regions belonging to the same metastasis showed different TMB values: coring A and C had lower clonal TMB of 8 mut/MB while coring B displayed 16 mut/MB (Figure 6C). At subclonal level, the 3 TMB values were different, thus suggesting that heterogeneity has a relevant role in the TMB evaluation by tissue biopsy analysis (Figure 6C). Of note, genetic signature analysis confirmed that the molecular effect of TMZ was clonal for coring B (Figure 6D) with higher TMB, while the effect was evident only at subclonal level for regions A and C (Figure 6D). Venn diagrams of all genetic alterations demonstrated that corings A and C were identical at clonal level and these were a subset of the coring B (Figure 6E, left). On the other hand, at subclonal level, all three regions displayed elevated heterogeneity, maintaining a core of 202 common mutations (Figure 6E, right).

Clinical and molecular monitoring of patients treated with pembrolizumab after TMZ priming

The planned accrual of 20 patients to be treated with immunotherapy was disrupted by the COVID19 pandemic. Since the trial proved lengthy, we present here the first six patients treated with the anti-PD-1 pembrolizumab. Although there were no objective partial or complete responses according to the iRECIST definition (70), four patients had sustained SD as best response, lasting for >2 years, 6.5 and 5.5 months (AR02007, AR01015 and AR03047, respectively), while the patient (AR01034) achieving SD died of myocardial infarction while still progression-free at 2.9 months (Figure 7A). We thus observed a disease control in 4 of 6 heavily pre-treated cases, corresponding to a disease control rate (DCR) of 67%. To exclude that DCR could be ascribed to differences in growth kinetics of individual tumors, independently of TMZ, we calculated the growth modulation index (GMI) of the overall treatment strategy in each patient, allowing intra-patient comparison of previous Time to Progression intervals (TTPs) (71, 72). Interestingly, the median GMI was 1.8 [range 1.2-7.0] and all patients treated with TMZ and pembrolizumab achieved a GMI > 1.33 (cut-off of clinical meaningfulness (73)) with exception of patient AR01034 who died for other causes without signs of progression (Figure 7B).
To longitudinally monitor the effect of pembrolizumab on TMZ-primed patients, we performed serial molecular profiling of plasma collected at multiple time-points during

anti-PD1 treatment (Figure 7C and Supplementary Figure S6A). In AR02007, who had long-lasting SD, we found that bTMB (at both clonal and subclonal level), increased during TMZ-based priming treatment, declining after pembrolizumab treatment (Cycle 10: clonal bTMB from 57 to 17 mut/MB; subclonal bTMB from 2276 to 50 mut/MB) with a stabilization of the clonal bTMB (at Cycles 10, 20 and 34, bTMB clonal was always 17 mut/MB) and with bTMB subclonal returning approximately at baseline (pre-priming) levels in the last analyzed timepoint (subclonal bTMB from 26 mut/MB before the TMZ priming to 27 mut/MB after pembrolizumab discontinuation (Figure 7C)). Of note, bTMB high to low switch (at clonal and subclonal level) is also accompanied by the emergence and decline of the *MSH6* p.T1219I variant and other MMR gene mutations, suggesting that the efficacy of ICB treatment was predominantly directed against the MMRd fraction of the tumor. Longitudinal plasma analysis of the AR02007 patient also showed that *MSH6* p.T1219I emerged in blood upon TMZ treatment, declined during immunotherapy treatment and eventually disappears after 9 pembrolizumab cycles (Figure 7C). Conversely, in other patients achieving shorter SD as best response to pembrolizumab (AR01015 and AR03047) or experiencing progressive disease (AR01013 and AR01052), no VAF decrease of trunk/driver mutations was observed. Longitudinal ctDNA analysis in these patients highlighted that bTMB clonal was stable during pembrolizumab treatment (AR03047: from 6 to 7 Mut/MB; AR01015: from 14 to 14 Mut/MB; AR01013: from 4 to 5 Mut/MB; AR01052 from 6 to 7 Mut/MB) (Supplementary Figure S6A) while longitudinal bTMB subclonal increased along anti-PD-1 treatment in 4/6 cases (AR03047, AR01015, AR01013 and AR01052).

In a subset of the cases, CEA levels were monitored at multiple longitudinal timepoints (baseline, best-response and progression/treatment discontinuation) during both priming and immunotherapy. In the two patients achieving durable SD, the CEA levels accordingly decreased (AR02007) or remained unchanged compared with baseline (AR01015), while in two patients displaying short-lived SD, CEA either increased (AR03047) or was not altered at baseline and remained unaltered until progression (AR01034). In the two remaining patients who had PD as best response, CEA levels rapidly increased as expected (Figure S6B). In AR01034, CEA levels were not indicative as they were within the range of physiological values (cut-off: 5 ng/ml). In the other patients, the trend of CEA levels paralleled the trend of tumor load during treatment (as assessed by radiological evaluation by RECIST 1.1

criteria). As expected, specific increase of CEA levels was observed concurrently with progressive disease. A specific response in CEA levels during pembrolizumab treatment was observed only in AR02007 patient in which long-SD is accompanied by shrinkage of the metastatic lesions (Supplementary Figure S6B).

DISCUSSION

In most solid tumors, TMB levels have been shown to correlate with response to ICB (74). Indeed, the FDA has approved a cancer type-agnostic use of the anti PD-1 pembrolizumab in patients with a TMB ≥ 10 mutations/megabase (50, 74). Unfortunately, the vast majority of mCRC patients are MMRp, display a low TMB and do not respond to anti-PD(L)-1 therapies. The ARETHUSA trial was designed to test the concept that pharmacological inactivation of MMR pathways could be clinically actionable. Accordingly, ARETHUSA is a *proof-of-concept* phase II trial, testing whether a dynamic TMB increase in MSS mCRC can be obtained by therapeutic priming with the alkylating agent TMZ, potentially favoring response to ICB. This unconventional approach is based on our prior preclinical evidence showing that TMZ is active against mCRC (45, 46) and also targets the DNA repair processes resulting in both TMB and neoantigens increase in tumor cells (44). ARETHUSA was designed as a 2-step study taking advantage of our previous knowledge that optimal selection for efficacy of TMZ in mCRC is achieved by a two-layer molecular assessment of MGMT inactivation involving IHC and methylation assays (49). In the first phase of the trial, TMZ is used for both its direct antitumor effect, and as a 'pharmacological primer' by inactivating MMR genes thus leading to increased mutational burdens such as SNVs and indels. These could, in turn, lead to the generation of neoepitopes, thus sparking immune surveillance and boosting response to ICB.

In the initial analysis reported here we studied how TMZ treatment affects the genome of MGMT-negative *RAS* mutated mCRC.

First, we found that the specific TMZ-signature 11 emerges in post-TMZ treatment samples of mCRC patients and the effect is dependent upon the number of cycles, suggesting that a minimum exposure level/time is required for detection of the TMZ genomic scar.

Second, we report that only patients whose tumors carried the characteristic TMZ-signature developed high subclonal or clonal TMB levels. However, post TMZ TMB measured in tissue from a single metastatic site might fail to fully capture the heterogeneity of inter- and even intra-metastasis response to TMZ. Indeed, our

results suggest that the molecular effect of TMZ differentially affects distinct regions of the same lesion. Therefore, to more comprehensively capture the mutational impact of TMZ more comprehensively, we thus measured TMB in ctDNA and found it largely comparable to the subclonal TMB calculated by WES data obtained by tissue biopsy. On the other hand, bTMB was influenced by ctDNA levels (see Supplementary Table S2 and Figure S4B). This finding tallies with the evidence that different tumors and/or metastatic sites may have a different ctDNA release capacity, thus potentially affecting bTMB analysis. Indeed, it was recently reported that both lung and peritoneum mCRC lesions have significantly lower maximum allele frequencies and lower number of cancer specific variants in blood as compared to patients with lesion in other metastatic sites, like the liver (64). Singularly, neither TMB (from tissue) nor bTMB (from blood) analysis are sufficient alone to correctly stratify the patients. Collectively these results suggest that an integrated analysis coupling both plasma and tissue TMB evaluation is more informative. Longitudinal CEA levels may correlate with disease burden in some patients, but they do not capture the clonal dynamics triggered by TMZ treatment.

Third, we revealed that the TMZ mutational signature is heralded by the presence in plasma and tissue of the p.T1219I variant of the MMR gene *MSH6*. Additional mutations in *MSH6* were also found exclusively in both tissue and plasma post TMZ treatment, further strengthening this association. In addition, we have highlighted the *MSH6* p.T1219I variant as a potential marker for TMZ molecular efficacy in CRC. Confirmation of this variant as a predictive marker of response should be assessed in further validation studies. In support of the 'predictive' relevance of this variant, we did not observe the p.T1219I in patients where mutational signature 11 was absent post-TMZ treatment whilst it emerged in 94% of patients who benefited from TMZ treatment (16/17 = 94%). Further analyses corroborated this notion by revealing additional mutations in *MSH6* detected only in both tissue and ctDNA post-TMZ samples. Notably, all *MSH6* SNVs (100%) are related to the nucleotide contexts favored by signature 11.

Tantalizingly, one of the patients (AR02007) who reached a major TMB increase upon TMZ priming and then treated with pembrolizumab achieved disease control lasting for over 2 years. The AR02007 disease stabilization was tracked in blood by following specific trunk/driver mutations (*TP53* and *KRAS*) in longitudinal plasma

samples collected during treatments. This analysis highlighted the onset of *MSH6* p.T1219I variant after TMZ-based treatment and its decline, until disappearing, during ICB treatment. Of interest, in this patient the trend of the *MSH6* variant mirrors that of bTMB (at both clonal and subclonal level).

While it is conceivable that pharmacological inactivation of the MMR pathway by TMZ is related to increased mutational and neoantigen burdens and therefore to immune modulation, other mechanisms linking DNA damage and immune surveillance also exists (75). These include, but are not limited to, activation of the cGAS/STING pathway by cytosolic DNA, as recently reported for MMRd tumors (76). It is therefore plausible that inactivation of MMR upon pharmacological treatment with alkylating agents such as TMZ could also trigger intracellular signaling pathways leading to innate antitumor immunity.

A major limitation of our current analysis is that owing to the limited amount of tissue available through post-TMZ biopsies, the investigations were limited to WES for TMB measurements as we were unable to perform other analyses on the same samples. In this regard, future studies may investigate whether TMZ treatment can induce up-regulation of PD-L1, and increased infiltration of IFNγ+CD8+ T cells in human tumors, as previously observed in animal models (44). Another limitation of our approach is the narrow, though existing, anti-tumor TMZ activity. We are planning to address this aspect by combinatorial studies in which TMZ will be associated with more active therapeutic regimens.

Finally, while we recognize that no conclusions can be made at this junction on the clinical utility of TMZ as an immune chemo-sensitizer, the wealth of pharmacodynamic data we produced as well as the GMI results are suggestive. The surprisingly long median TTP (the expected TTP in this population of mCRC patients pre-treated with 3 or more lines of therapies is ~ 2 months (77, 78)), is unlike due to the growth kinetics of the patients' cancer as suggested by the GMI > 1 values in all cases. Furthermore, our findings support the recent results from the MAYA trial (NCT03832621) in MGMT methylated MSS mCRC patients (79). MAYA, differently to ARETHUSA, exploited a 2-month TMZ priming phase, which was followed in absence of PD by a combinatorial approach made of TMZ with low-dose ipilimumab

plus nivolumab. Consistently with the ARETHUSA patient cohort, approximately one fourth of the MAYA patients primed with TMZ eventually received immunotherapy (79). The primary endpoint of 8-months PFS rate in MAYA trial was met, reaching a notable 32% compared to an historical 5%, and median PFS was 7.1 months possibly favored by the use of an anti-PD1 and anti-CTLA4 combination or to an earlier start of immunotherapy (80, 81). Interestingly enough, the analysis of tumor-paired biopsies, albeit limited to the TMB assessment and conducted only in four patients, showed an acquired high TMB (79).

In summary, we provide a *proof-of-concept* that the inactivation of genes involved in DNA repair can be achieved pharmacologically with TMZ treatment, while offering potential clinical benefit to *MGMT* methylated *RAS* mutant mCRC patients refractory to standard of care treatments. We also show that the priming process can be monitored in tissue and blood samples, providing initial evidence of a blood biomarker used to effectively measure the effectiveness of MMR inactivation. Although the ARETHUSA trial is not completed yet, the multidimensional translational analyses presented here show that increased mutational burdens can be achieved by pharmacological modulation in *RAS* mutant MSS CRCs with an initial low baseline TMB. Additional studies are needed to confirm the relevance and applicability of this approach for the treatment of *RAS* mutant MSS mCRC.

METHODS

The ARETHUSA trial

Institutional review boards of all participating institutions (Niguarda Cancer Center, Grande Ospedale Metropolitano Niguarda, Milan; Fondazione IRCCS Istituto Nazionale dei Tumori, Milan; HUMANITAS Research Hospital, Rozzano and IEO Istituto Europeo di Oncologia, Milano), approved the study procedure. All patients provided written informed consent for participation to the study and associated procedures. The study was conducted in accordance with the principles of the Declaration of Helsinki and the International Conference on Harmonization and Good Clinical Practice guidelines. The ARETHUSA trial (NCT03519412; EudraCT number 2018-001441-14) is sponsored by IFOM and has been approved by local Ethical Committee and Italian Competent Authority (AIFA) on 29/10/2018.

In the Screening Phase of ARETHUSA (NCT03519412), *RAS* extended (*KRAS* or *NRAS*, exons 2, 3, 4) mutant MSS/MMRp mCRC patients were tested for MGMT status in tissue by immunohistochemistry (IHC) (49) and methyl-BEAMing (see below, Methyl-BEAMing assay paragraph). Patients with MGMT IHC staining negative and methylated *MGMT* promoter were enrolled in the Priming phase and underwent treatment with oral TMZ (150 mg/m2/day; day1-5 q28, Figure 1) until disease progression or unacceptable toxicity. Disease progression was determined according to RECIST v1.1 (82).

At disease progression or treatment discontinuation, a mandatory biopsy was performed to evaluate the TMB. Only MSS/MMRp patients with tumor mutational load ≥ 20 mutations/Mb post TMZ treatment were enrolled in the Immunotherapy phase and received intravenous anti-PD1 blockade by pembrolizumab monotherapy (200mg q3w) until disease progression, unacceptable toxicity or up to 24 months in patients without disease progression (Figure 1).

Of note, two liquid biopsies for the experimental NGS-based determination of the molecular profiling and tumor mutational burden in the blood (bTMB) were collected pre- and post-treatments (Figure 1).

Methyl-BEAMing assay

Five hundred nanograms of DNA were used for bisulfite conversion using the EZ DNA methylation gold kit (Zymo Research), following manufacturer's protocol, with final elution in 70 µL. Bisulfite converted DNA was assessed via methyl-BEAMing for the methylation status of MGMT gene. Methyl-BEAMing analysis is a multistep digital PCR based technique (83). A first amplification allows the enrichment of the locus of interest and is carried out using tagged-primers. Amplicons are then diluted (1/16000) and re-subjected to PCR amplification using the tag and tag-coated-beads. The second round of amplification is performed in emulsion allowing physical separation and independent amplification of the different templates. PCR mixes are prepared according to conditions described (84). Next, emulsion is broken using alcohol-based buffers (isopropanol/butanol) and amplicons are hybridized with fluorescent probes specific for the methylated or unmethylated bisulfite converted templates. Fluorescence is then assessed on an Accuri C6 flow cytometer (BD) using the filters previously established with controls (scale of methylation). The percentage of methylation is calculated dividing the number of methylated specific events by the sum of methylated plus unmethylated specific events. A minimum of 200 cumulative events (methylated + unmethylated) is required for a result to be considered valid. Quantification ability and linearity of the Methyl-BEAMing assay was previously tested with a scale made of template corresponding to the fully methylated or unmethylated bisulfite converted sequence (84). Threshold for calling a sample positive was setup at 34.5% based on expected clinical benefit observed in MGMT IHC negative patients reported (49).

Cell lines and in vitro drug treatments

SKCO1 and SW620 CRC cell lines are part of a large dataset that we previously described (85). Cells were routinely supplemented with FBS 10% 2mM L-glutamine, antibiotics (100U/mL penicillin and 100 mg/mL streptomycin) and grown in a 37°C and 5% CO2 air incubator. Cells were routinely screened for absence of Mycoplasma contamination using the Venor® GeM Classic kit (Minerva biolabs). The identity of each cell line was checked using the PowerPlex® 16 HS System (Promega), through Short Tandem Repeats (STR) tests at 16 different loci (D5S818, D13S317, D7S820, D16S539, D21S11, vWA, TH01, TPOX, CSF1PO, D18S51, D3S1358, D8S1179, FGA, Penta D, Penta E, and amelogenin). Amplicons from multiplex PCRs were separated by capillary electrophoresis (3730 DNA Analyzer,

Applied Biosystems) and analyzed using GeneMapper v.3.7 software (Life Technologies).

Cells were cultured with 100μM of TMZ until they acquired resistance as previously described (44). When resistance seemed acquired, a scalar concentration of drug was assessed to verify the increased in IC50 compared to parental. At this point, identity of the cell line was checked through STR profiling (Promega). Then, in order to evaluate the mutational signature acquired post treatment refractoriness, two million resistant cells were seeded in 10 cm dish in media without drug for 21 days, then cells were collected and DNA was extracted for WES.

NGS workflow and WES data generation

QIAmp DNA and Blood mini kit (QIAGEN, Hilden, Germany) were used for DNA extraction from PBMC and fresh tissue. The preparation was performed following manufacturer's protocol. Starting from 200 ng of DNA from fresh tissue/PBMC, NGS libraries were prepared by means of Nextera DNA Flex Library Prep kit (Illumina Inc., San Diego, CA, USA), according to the manufacturer's protocol. Subsequent whole exome target enrichment has been performed following IDT xGen protocol (xGen Hybridization and Wash Kit, xGen Universal Blockers-NXT Mix, xGen Exome Research Panel v2; IDT, Inc. Coralville, Iowa, USA). Quality of libraries has been checked with High-Sensitivity DNA assay kit (Agilent Technologies, Santa Clara, CA). Library preparation, enrichment of whole exome regions, and sequencing of patient's samples were performed by Cogentech Società Benefit srl.

NGS libraries for cell line samples were prepared starting with 150ng of DNA and processed with Illumina DNA Prep with Enrichment and Exome Panel 45Mb (Illumina Inc., San Diego, CA, USA), according to the manufacturer's protocol. After fragmentation of gDNA with transposon enzyme and subsequent PCR to introduce unique sample indexes, DNA fragments' size distribution was assessed using the 2100 Bioanalyzer with a High-Sensitivity DNA assay kit (Agilent Technologies, Santa Clara, CA). Equal amounts of DNA libraries were pooled and subjected to targeted panel hybridization capture.

Final libraries were sequenced on NextSeq sequencer 500 or 550 DX (Illumina Inc., San Diego, CA, USA).

Genetic Analysis of Tissue: mutational profiling and TMB analysis

“Fastq files” were generated using bcl2fastq command and the high-depth sequencing data was obtained (Supplementary Table S1). Fastq files were processed using the genomic analysis workflow for precision oncology as earlier described (67, 68). BWA-mem algorithm was used to map reads to the human genome version 19 (hg19) and PCR duplicates were removed using the RMDUP command in the SAMtools bioinformatic suite. To delete NGS artifacts (86) reads having more than 3 different mismatches and bases with quality PhredScore < 30 were not considered in the mutations calling step. Mutations supported only by alteration fallen in the first/last reads position were filtered and strand bias correction was applied as earlier described (68). Pindel tool was used for the indels calling. After filtering step (where NGS artifacts were filtered out), a median depth 376X, coverage ≥ 96.82% at 100X depth with a median of 124 million reads per sample was obtained (Supplementary Table S1).

Alignments from PBMC and tissue tumor samples were compared to identify mutations/indels in tumor and matched normal samples. Germline mutations were common to both samples, while somatic alterations were present only in tumor. For cell lines analysis, mutation calling was performed using hg19 as reference and filtering out all mutations reported in the dbSNP (v147). In the section “Identification of the TMZ signature in CRC cells treated with TMZ”, in order to consider only the acquired mutations, two independent sequencing of the same parental cell line were performed in order to use one parental cell line as reference.

All the VAFs reported in the text were adjusted using the copy number variation data (Tumor vs Germinal). In order to verify the diploidy of the germinal DNA of each patient, the ploidy analysis was performed. Large copy number alterations were identified by the aneuploidy score (AS), defined as the sum of the number of altered chromosome arms (87). All chromosomes of 21 germinal PBMC obtained the lowest values (score 0, all arms of autosomal chromosomes were diploid). Focal ploidy was identified based on copy number analysis of germline DNA from PBMC in comparison with a metanormal built from 21 PBMC sequenced using the same “wet” procedures. This comparison was used for correction of different probes affinity.

Finally, tumor focal gene copy number variations analysis was performed in the matched samples (Tumor vs Germinal) for each patient. Gene copy number (CN)

was calculated as the ratio of median gene depth and the median depth of all genes in the whole exome. For each gene, the copy number alteration (CNA) was calculated as the ratio between the CN of normal tissue and CN of the same gene in the tumor samples as previously reported (67, 68). Tumor copy number was considered altered when the log2 value was higher than 1 or lower than -1. On the basis of the copy number variation, VAF of all the mutations fallen into altered regions were then normalized. Overall, as expected, no gene amplifications or deep deletions were reported in the tumor tissue biopsy collected after TMZ treatment. In detail, only slight and focal copy number increase/decrease were reported in the tumor patient cohort with a median value of 0.00696011% (or mean of 0.1820%) of altered genomic regions.

TMB was calculated from WES data taking into consideration nucleotide variants with 5% significance level obtained with a Fisher test and supported by a minimum of 4 mutated reads in regions with a minimum depth of 5X. We considered only mutations with adjusted allele frequency ≥ 10% for clonal analysis and ≥ 1% for subclonal analysis, excluding mutations annotated in dbSNP (v147). All data were normalized on the real target regions as previously described (6, 44, 68, 88).

We performed another type of normalization using a sliding cutoff (not the 10% fixed cutoff) in order to check if another method of cell purity calculation could influence our clonal/subclonal results. In detail, we normalized the TMB on the basis of the purity calculation as described in (89). The clonal/subclonal TMB and mutational signatures results were also confirmed using this alternative approach based on (89), with respect to manuscript method (data not shown). In conclusion, using an alternative method the tumors patients' stratification in A, B1 and B2 subtypes based on clonal/subclonal results was confirmed.

Mutational Signature Analysis

Only alterations with fractional abundance ≥ 10% were used for clonal analysis while alterations with fractional abundance ≥ 1% were used for subclonal analysis. The matrix with mutation contexts was build using sigprofilerMatrixGenerator (90).

Using the information of somatic SNVs in the matrix, a series of mutational profiles were extracted, and genetic signatures were calculated using the MuSiCa tool (91) and Mutational Patterns package (59). COSMIC signature references v. 2.0, v 3.0 and v. 3.2 were used for the fitting in the mutational signature analysis. For clonal analysis in five cases (AR02071, AR01032, AR01014, AR01069 and AR02064), the number of mutations was not sufficient to perform the supported mutational analysis (cosine similarity lower than 0.9) and these five samples were excluded. The clonal mutations (with VAF ≥ 10%) were not enough to perform signature analysis in some samples of the SW620/SKCO1 cell lines.

Cosine similarity between two vectors of the same length was calculated using the MUSICA (91) and Mutational Patterns tools (59). The cosine was used to evaluate the similarity between the original mutational profile (obtained by the mutations identified in the sample) and the reconstructed mutational profile based on the optimal linear combination of all COSMIC signatures identified after fitting (59, 60). All mutations with allelic frequencies ≥ 1% (for subclonal analysis) and ≥ 10% (for clonal analysis) were also used to build a distance matrix that was starting point to build the agglomerative hierarchical clustering. The “Cluster” package of the R software (freely available at www.r-project.org) and unweighted pair group average method – UPGMA -- were used.

For the enrichment analysis of the Signature 11 contexts in *APC* and MMR genes, we started dividing the nucleotide sequence of each gene (sliding window) in the three nucleotides (triplets) contexts that then were extracted to considering the fractional abundance of each context in the genes. The following contexts (ACC; ACT; AGA; AGG; AGT; CAA; CCC; CCG; CCT; CGG; GCA; GCC; GGA; GGC; GGG; GGT; TCA; TCC; TGA; TGC; TGG) were considered “favored by Signature 11” on the base of the mutation probability reported for Signature 11 (57).

TMB/Signature detection in preclinical models

To simulate mixed population of CRC cell models (sensitive and resistant to TMZ) “*in-silico*” NGS databases were established. FastQ files for each population were created using different percentage of sequencing reads obtained by 100% TMZ-

Sensitive (TMZ-S) parental and 100% TMZ-resistant (TMZ-R) cells from sequencing data by SW620 and SKCO1 cell lines. The six populations were composed as follows: 100% TMZ-R (1), 50% TMZ-R + 50% TMZ-S (2), 25% TMZ-R+ 75% TMZ-S (3), 12.5% TMZ-R + 87.5% TMZ-S (4), 6.25% TMZ-R and 93.75% TMZ-S (5) and 100% TMZ-S (6). A fixed number of 100.663.296 reads was always used as the total number of reads, while the ratio of reads derived from Resistance/Sensitive cells. With this method we created the paired fastQ files for each mixed population. Starting from *in-silico* fastQ files, each population was then analyzed as previously reported.

ctDNA mutational profiling and bTMB analysis

Whole-blood samples were collected in K2-EDTA tubes before patients started temozolomide treatment (baseline, pre-TMZ) and/or at the time of disease progression (post-TMZ). Plasma was isolated from the cellular component and frozen. Frozen plasma samples were shipped to Guardant Health for cfDNA extraction and mutational profiling. Extracted cfDNA was analyzed using the GuardantOMNI research-use only (RUO) NGS assay (Guardant Health, Inc) to identify single nucleotide variations (SNVs), indels, gene fusions, copy number variants, microsatellite status, and blood tumor mutational burden (bTMB) across a 2.145 Mb panel. Blood TMB (bTMB) was reported as variations per megabase (mut/Mb) by the GuardantOMNI algorithm (63), which includes all somatic synonymous and nonsynonymous SNVs and indels filtering out and excluding germline, clonal hematopoiesis of indeterminate potential (CHIP), known driver and resistance variations. Statistical adjustment for sample-specific tumor shedding and molecular coverage, as well as normalization by panel size, were performed (63). Further details were available at (63).

bTMB was further divided in the clonal (using the sliding cutoff of 10% of the tumor content identified in the sample) and subclonal counterpart.

Growth modulation Index calculation

The growth modulation index (GMI) was defined as previously described (92). Briefly, comparison of Progression-Free survival (PFS) on overall ARETHUSA strategy treatment (TMZ and pembrolizumab; PFS_n) versus PFS on prior therapy

(PFS_{n-1}) was performed. A GMI >1.33, i.e., an increase in the PFS_n/PFS_{n-1} ratio of 30%, was considered as clinically meaningful (72).

Statistical analysis

Statistical analysis was performed using R (version 3.6.3 and 4.0.3). The individual statistical tests used are specified in the relevant Results section and Figures legends.

Spearman rank correlation was performed between the number of mutations/megabase induced by TMZ Signature (normalized_score_SBS11 * TMB from only SNVs) and TMZ courses in patients (Figure 3C, p-value = 2.535e-5 and Cor = 0.7847). Wilcoxon rank sum test was used to compare bTMB in matched pre-post TMZ plasma samples (p-value = 0.002443, Figure 4DE). Pearson's product-moment correlation (p-value = 2.34e-12, Supplementary Figure S5A) was used for the correlation between TMB obtained by cell-based and *in-silico* analyses.

Data and Software Availability

Bioinformatic codes are available at https://bitbucket.org/irccit/idea/src/master/.

Human sequencing data are available at EGAS00001002694 (EGA; https://www.ebi.ac.uk/ega/home), PRJEB33045 and PRJEB46380 (ENA: https://www.ebi.ac.uk/ena/browser/search).

Acknowledgements

We thank all the patients and their families, we also thank the members of the Molecular Oncology laboratory at the Candiolo Cancer Institute, FPO – IRCCS and at the Department of Oncology, University of Torino for critically reading the manuscript.

Author Contributions

G.C., S.M., A.S.B., S.S., F.D.N. and A.Bardelli conceived the study. A.S.B., S.S., F.P., N.P., A.A., F.T., M.G.Z. G.C. and F.M. performed clinical studies, obtained tissue samples and performed patient data analysis. G.C. conducted bioinformatics data analyses. L.L and P.L. performed data analysis and monitoring. A.C. and L.I. provided clinical data and samples. M.M, L.B., A.Bartolini, P.B., V.P. E.V. and E.B. performed the experiments. G.G and P.P.V. contributed to data discussion. G.C.

G.M. F.D.N. and A.Bardelli wrote the manuscript. A.Bardelli, S.M., A.S.B., S.S. and F.D.N. supervised the study. All the authors read and approved the final manuscript.

REFERENCES

1. Siegel RL, Miller KD, Fuchs HE, Jemal A. Cancer Statistics, 2021. CA Cancer J Clin. 2021;71(1):7-33.
2. Sung H, Ferlay J, Siegel RL, Laversanne M, Soerjomataram I, Jemal A, et al. Global Cancer Statistics 2020: GLOBOCAN Estimates of Incidence and Mortality Worldwide for 36 Cancers in 185 Countries. CA Cancer J Clin. 2021;71(3):209-49.
3. Yoshino T, Arnold D, Taniguchi H, Pentheroudakis G, Yamazaki K, Xu RH, et al. Pan-Asian adapted ESMO consensus guidelines for the management of patients with metastatic colorectal cancer: a JSMO-ESMO initiative endorsed by CSCO, KACO, MOS, SSO and TOS. Ann Oncol. 2018;29(1):44-70.
4. Benson AB, Venook AP, Al-Hawary MM, Arain MA, Chen YJ, Ciombor KK, et al. Colon Cancer, Version 2.2021, NCCN Clinical Practice Guidelines in Oncology. J Natl Compr Canc Netw. 2021;19(3):329-59.
5. Sartore-Bianchi A, Trusolino L, Martino C, Bencardino K, Lonardi S, Bergamo F, et al. Dual-targeted therapy with trastuzumab and lapatinib in treatment-refractory, KRAS codon 12/13 wild-type, HER2-positive metastatic colorectal cancer (HERACLES): a proof-of-concept, multicentre, open-label, phase 2 trial. Lancet Oncol. 2016;17(6):738-46.
6. Siravegna G, Lazzari L, Crisafulli G, Sartore-Bianchi A, Mussolin B, Cassingena A, et al. Radiologic and Genomic Evolution of Individual Metastases during HER2 Blockade in Colorectal Cancer. Cancer Cell. 2018;34(1):148-62.e7.
7. Kopetz S, Grothey A, Yaeger R, Van Cutsem E, Desai J, Yoshino T, et al. Encorafenib, Binimetinib, and Cetuximab in. N Engl J Med. 2019;381(17):1632-43.
8. Mauri G, Bonazzina E, Amatu A, Tosi F, Bencardino K, Gori V, et al. The Evolutionary Landscape of Treatment for. Cancers (Basel). 2021;13(1).
9. Siena S, Di Bartolomeo M, Raghav K, Masuishi T, Loupakis F, Kawakami H, et al. Trastuzumab deruxtecan (DS-8201) in patients with HER2-expressing metastatic colorectal cancer (DESTINY-CRC01): a multicentre, open-label, phase 2 trial. Lancet Oncol. 2021.
10. Ganesh K, Stadler ZK, Cercek A, Mendelsohn RB, Shia J, Segal NH, et al. Immunotherapy in colorectal cancer: rationale, challenges and potential. Nat Rev Gastroenterol Hepatol. 2019;16(6):361-75.
11. Koopman M, Kortman GA, Mekenkamp L, Ligtenberg MJ, Hoogerbrugge N, Antonini NF, et al. Deficient mismatch repair system in patients with sporadic advanced colorectal cancer. Br J Cancer. 2009;100(2):266-73.
12. Sinicrope FA, Sargent DJ. Molecular pathways: microsatellite instability in colorectal cancer: prognostic, predictive, and therapeutic implications. Clin Cancer Res. 2012;18(6):1506-12.
13. Jiricny J. The multifaceted mismatch-repair system. Nat Rev Mol Cell Biol. 2006;7(5):335-46.
14. Cohen R, Rousseau B, Vidal J, Colle R, Diaz LA, André T. Immune Checkpoint Inhibition in Colorectal Cancer: Microsatellite Instability and Beyond. Target Oncol. 2020;15(1):11-24.
15. Network CGA. Comprehensive molecular characterization of human colon and rectal cancer. Nature. 2012;487(7407):330-7.
16. Rospo G, Lorenzato A, Amirouchene-Angelozzi N, Magrì A, Cancelliere C, Corti G, et al. Evolving neoantigen profiles in colorectal cancers with DNA repair defects. Genome Med. 2019;11(1):42.

17. Llosa NJ, Cruise M, Tam A, Wicks EC, Hechenbleikner EM, Taube JM, et al. The vigorous immune microenvironment of microsatellite instable colon cancer is balanced by multiple counter-inhibitory checkpoints. Cancer Discov. 2015;5(1):43-51.
18. Gryfe R, Kim H, Hsieh ET, Aronson MD, Holowaty EJ, Bull SB, et al. Tumor microsatellite instability and clinical outcome in young patients with colorectal cancer. N Engl J Med. 2000;342(2):69-77.
19. André T, Shiu KK, Kim TW, Jensen BV, Jensen LH, Punt C, et al. Pembrolizumab in Microsatellite-Instability-High Advanced Colorectal Cancer. N Engl J Med. 2020;383(23):2207-18.
20. Lenz HJ, Van Cutsem E, Luisa Limon M, Wong KYM, Hendlisz A, Aglietta M, et al. First-Line Nivolumab Plus Low-Dose Ipilimumab for Microsatellite Instability-High/Mismatch Repair-Deficient Metastatic Colorectal Cancer: The Phase II CheckMate 142 Study. J Clin Oncol. 2022;40(2):161-70.
21. Le DT, Kim TW, Van Cutsem E, Geva R, Jäger D, Hara H, et al. Phase II Open-Label Study of Pembrolizumab in Treatment-Refractory, Microsatellite Instability-High/Mismatch Repair-Deficient Metastatic Colorectal Cancer: KEYNOTE-164. J Clin Oncol. 2020;38(1):11-9.
22. Overman MJ, Lonardi S, Wong KYM, Lenz HJ, Gelsomino F, Aglietta M, et al. Durable Clinical Benefit With Nivolumab Plus Ipilimumab in DNA Mismatch Repair-Deficient/Microsatellite Instability-High Metastatic Colorectal Cancer. J Clin Oncol. 2018;36(8):773-9.
23. Aisha Ghaus AP, Victoria Murdock, Hala Shareef, Leslie M. Samuel, Sally Clive, Fay Tough, Lisa Jane Rodgers. Real-world experience of pembrolizumab in microsatellite instability-high CRC: A Scottish multicenter analysis.: Journal of Clinical Oncology; 2022. p. 54-.
24. Rousseau B, Foote MB, Maron SB, Diplas BH, Lu S, Argilés G, et al. The Spectrum of Benefit from Checkpoint Blockade in Hypermutated Tumors. N Engl J Med. 2021;384(12):1168-70.
25. Le DT, Uram JN, Wang H, Bartlett BR, Kemberling H, Eyring AD, et al. PD-1 Blockade in Tumors with Mismatch-Repair Deficiency. N Engl J Med. 2015;372(26):2509-20.
26. Oki E, Makiyama A, Miyamoto Y, Kotaka M, Kawanaka H, Miwa K, et al. Trifluridine/tipiracil plus bevacizumab as a first-line treatment for elderly patients with metastatic colorectal cancer (KSCC1602): A multicenter phase II trial. Cancer Med. 2021;10(2):454-61.
27. Bourhis J, Stein A, Paul de Boer J, Van Den Eynde M, Gold KA, Stintzing S, et al. Avelumab and cetuximab as a therapeutic combination: An overview of scientific rationale and current clinical trials in cancer. Cancer Treat Rev. 2021;97:102172.
28. Cousin S, Cantarel C, Guegan JP, Gomez-Roca C, Metges JP, Adenis A, et al. Regorafenib-Avelumab Combination in Patients with Microsatellite Stable Colorectal Cancer (REGOMUNE): A Single-arm, Open-label, Phase II Trial. Clin Cancer Res. 2021;27(8):2139-47.
29. Chen EX, Jonker DJ, Loree JM, Kennecke HF, Berry SR, Couture F, et al. Effect of Combined Immune Checkpoint Inhibition vs Best Supportive Care Alone in Patients With Advanced Colorectal Cancer: The Canadian Cancer Trials Group CO.26 Study. JAMA Oncol. 2020;6(6):831-8.
30. Marmorino F, Boccaccino A, Germani MM, Falcone A, Cremolini C. Immune Checkpoint Inhibitors in pMMR Metastatic Colorectal Cancer: A Tough Challenge. Cancers (Basel). 2020;12(8).

31. Stupp R, Brada M, van den Bent MJ, Tonn JC, Pentheroudakis G, Group EGW. High-grade glioma: ESMO Clinical Practice Guidelines for diagnosis, treatment and follow-up. Ann Oncol. 2014;25 Suppl 3:iii93-101.
32. Pavel M, Öberg K, Falconi M, Krenning EP, Sundin A, Perren A, et al. Gastroenteropancreatic neuroendocrine neoplasms: ESMO Clinical Practice Guidelines for diagnosis, treatment and follow-up. Ann Oncol. 2020;31(7):844-60.
33. Swetter SM, Thompson JA, Albertini MR, Barker CA, Baumgartner J, Boland G, et al. NCCN Guidelines® Insights: Melanoma: Cutaneous, Version 2.2021. J Natl Compr Canc Netw. 2021;19(4):364-76.
34. von Mehren M, Kane JM, Bui MM, Choy E, Connelly M, Dry S, et al. NCCN Guidelines Insights: Soft Tissue Sarcoma, Version 1.2021. J Natl Compr Canc Netw. 2020;18(12):1604-12.
35. Nabors LB, Portnow J, Ahluwalia M, Baehring J, Brem H, Brem S, et al. Central Nervous System Cancers, Version 3.2020, NCCN Clinical Practice Guidelines in Oncology. J Natl Compr Canc Netw. 2020;18(11):1537-70.
36. Casali PG, Bielack S, Abecassis N, Aro HT, Bauer S, Biagini R, et al. Bone sarcomas: ESMO-PaedCan-EURACAN Clinical Practice Guidelines for diagnosis, treatment and follow-up. Ann Oncol. 2018;29(Suppl 4):iv79-iv95.
37. Gronchi A, Miah AB, Dei Tos AP, Abecassis N, Bajpai J, Bauer S, et al. Soft tissue and visceral sarcomas: ESMO-EURACAN-GENTURIS Clinical Practice Guidelines for diagnosis, treatment and follow-up. Ann Oncol. 2021.
38. Hunter C, Smith R, Cahill DP, Stephens P, Stevens C, Teague J, et al. A hypermutation phenotype and somatic MSH6 mutations in recurrent human malignant gliomas after alkylator chemotherapy. Cancer Res. 2006;66(8):3987-91.
39. Yip S, Miao J, Cahill DP, Iafrate AJ, Aldape K, Nutt CL, et al. MSH6 mutations arise in glioblastomas during temozolomide therapy and mediate temozolomide resistance. Clin Cancer Res. 2009;15(14):4622-9.
40. Indraccolo S, Lombardi G, Fassan M, Pasqualini L, Giunco S, Marcato R, et al. Genetic, Epigenetic, and Immunologic Profiling of MMR-Deficient Relapsed Glioblastoma. Clin Cancer Res. 2019;25(6):1828-37.
41. Cahill DP, Levine KK, Betensky RA, Codd PJ, Romany CA, Reavie LB, et al. Loss of the mismatch repair protein MSH6 in human glioblastomas is associated with tumor progression during temozolomide treatment. Clin Cancer Res. 2007;13(7):2038-45.
42. Johnson BE, Mazor T, Hong C, Barnes M, Aihara K, McLean CY, et al. Mutational analysis reveals the origin and therapy-driven evolution of recurrent glioma. Science. 2014;343(6167):189-93.
43. Wang J, Cazzato E, Ladewig E, Frattini V, Rosenbloom DI, Zairis S, et al. Clonal evolution of glioblastoma under therapy. Nat Genet. 2016;48(7):768-76.
44. Germano G, Lamba S, Rospo G, Barault L, Magrì A, Maione F, et al. Inactivation of DNA repair triggers neoantigen generation and impairs tumour growth. Nature. 2017;552(7683):116-20.
45. Amatu A, Barault L, Moutinho C, Cassingena A, Bencardino K, Ghezzi S, et al. Tumor MGMT promoter hypermethylation changes over time limit temozolomide efficacy in a phase II trial for metastatic colorectal cancer. Ann Oncol. 2016;27(6):1062-7.
46. Amatu A, Sartore-Bianchi A, Moutinho C, Belotti A, Bencardino K, Chirico G, et al. Promoter CpG island hypermethylation of the DNA repair enzyme MGMT predicts clinical

response to dacarbazine in a phase II study for metastatic colorectal cancer. Clin Cancer Res. 2013;19(8):2265-72.
47. Pietrantonio F, Perrone F, de Braud F, Castano A, Maggi C, Bossi I, et al. Activity of temozolomide in patients with advanced chemorefractory colorectal cancer and MGMT promoter methylation. Ann Oncol. 2014;25(2):404-8.
48. Pietrantonio F, Randon G, Romagnoli D, Di Donato S, Benelli M, de Braud F. Biomarker-guided implementation of the old drug temozolomide as a novel treatment option for patients with metastatic colorectal cancer. Cancer Treat Rev. 2020;82:101935.
49. Sartore-Bianchi A, Pietrantonio F, Amatu A, Milione M, Cassingena A, Ghezzi S, et al. Digital PCR assessment of MGMT promoter methylation coupled with reduced protein expression optimises prediction of response to alkylating agents in metastatic colorectal cancer patients. Eur J Cancer. 2017;71:43-50.
50. Marabelle A, Fakih M, Lopez J, Shah M, Shapira-Frommer R, Nakagawa K, et al. Association of tumour mutational burden with outcomes in patients with advanced solid tumours treated with pembrolizumab: prospective biomarker analysis of the multicohort, open-label, phase 2 KEYNOTE-158 study. Lancet Oncol. 2020;21(10):1353-65.
51. Morano F, Corallo S, Niger M, Barault L, Milione M, Berenato R, et al. Temozolomide and irinotecan (TEMIRI regimen) as salvage treatment of irinotecan-sensitive advanced colorectal cancer patients bearing MGMT methylation. Ann Oncol. 2018;29(8):1800-6.
52. Pietrantonio F, Lobefaro R, Antista M, Lonardi S, Raimondi A, Morano F, et al. Capecitabine and Temozolomide versus FOLFIRI in RAS-Mutated, MGMT-Methylated Metastatic Colorectal Cancer. Clin Cancer Res. 2020;26(5):1017-24.
53. Alexandrov LB, Nik-Zainal S, Wedge DC, Aparicio SA, Behjati S, Biankin AV, et al. Signatures of mutational processes in human cancer. Nature. 2013;500(7463):415-21.
54. Alexandrov LB, Kim J, Haradhvala NJ, Huang MN, Tian Ng AW, Wu Y, et al. The repertoire of mutational signatures in human cancer. Nature. 2020;578(7793):94-101.
55. Davies H, Glodzik D, Morganella S, Yates LR, Staaf J, Zou X, et al. HRDetect is a predictor of BRCA1 and BRCA2 deficiency based on mutational signatures. Nat Med. 2017;23(4):517-25.
56. Nik-Zainal S, Alexandrov LB, Wedge DC, Van Loo P, Greenman CD, Raine K, et al. Mutational processes molding the genomes of 21 breast cancers. Cell. 2012;149(5):979-93.
57. Alexandrov LB, Nik-Zainal S, Wedge DC, Campbell PJ, Stratton MR. Deciphering signatures of mutational processes operative in human cancer. Cell Rep. 2013;3(1):246-59.
58. Petljak M, Alexandrov LB, Brammeld JS, Price S, Wedge DC, Grossmann S, et al. Characterizing Mutational Signatures in Human Cancer Cell Lines Reveals Episodic APOBEC Mutagenesis. Cell. 2019;176(6):1282-94.e20.
59. Blokzijl F, Janssen R, van Boxtel R, Cuppen E. MutationalPatterns: comprehensive genome-wide analysis of mutational processes. Genome Med. 2018;10(1):33.
60. Islam SMA, Alexandrov LB. Bioinformatic Methods to Identify Mutational Signatures in Cancer. Methods Mol Biol. 2021;2185:447-73.
61. Siravegna G, Mussolin B, Venesio T, Marsoni S, Seoane J, Dive C, et al. How liquid biopsies can change clinical practice in oncology. Ann Oncol. 2019;30(10):1580-90.
62. Di Nicolantonio F, Vitiello PP, Marsoni S, Siena S, Tabernero J, Trusolino L, et al. Precision oncology in metastatic colorectal cancer - from biology to medicine. Nat Rev Clin Oncol. 2021.

63. Si H, Kuziora M, Quinn KJ, Helman E, Ye J, Liu F, et al. A Blood-based Assay for Assessment of Tumor Mutational Burden in First-line Metastatic NSCLC Treatment: Results from the MYSTIC Study. Clin Cancer Res. 2021;27(6):1631-40.
64. Hideaki Bando YN, Hiroya Taniguchi, Manabu Shiozawa, Hisateru Yasui, Taito Esaki, Takashi Ohta, Tadamichi Denda, Taroh Satoh, Kentaro Yamazaki, Yu Sunakawa, Takeshi Kato, Masahiro Goto, Satoshi Yuki, Tomohiro Nishina, Eiji Oki, Eiji Shinozaki, Nobuhisa Matsuhashi, Masayuki Hata, Takayuki Yoshino. Impact of a metastatic site on circulating
tumor DNA (ctDNA) analysis in patients (pts) with metastatic colorectal
cancer (mCRC). Journal of Clinical Oncology; 2021. p. 3554-.
65. Misale S, Yaeger R, Hobor S, Scala E, Janakiraman M, Liska D, et al. Emergence of KRAS mutations and acquired resistance to anti-EGFR therapy in colorectal cancer. Nature. 2012;486(7404):532-6.
66. Oddo D, Siravegna G, Gloghini A, Vernieri C, Mussolin B, Morano F, et al. Emergence of MET hyper-amplification at progression to MET and BRAF inhibition in colorectal cancer. Br J Cancer. 2017;117(3):347-52.
67. Corti G, Bartolini A, Crisafulli G, Novara L, Rospo G, Montone M, et al. A Genomic Analysis Workflow for Colorectal Cancer Precision Oncology. Clin Colorectal Cancer. 2019;18(2):91-101.e3.
68. Crisafulli G, Mussolin B, Cassingena A, Montone M, Bartolini A, Barault L, et al. Whole exome sequencing analysis of urine trans-renal tumour DNA in metastatic colorectal cancer patients. ESMO Open. 2019;4(6).
69. Drost M, Tiersma Y, Glubb D, Kathe S, van Hees S, Calléja F, et al. Two integrated and highly predictive functional analysis-based procedures for the classification of MSH6 variants in Lynch syndrome. Genet Med. 2020;22(5):847-56.
70. Seymour L, Bogaerts J, Perrone A, Ford R, Schwartz LH, Mandrekar S, et al. iRECIST: guidelines for response criteria for use in trials testing immunotherapeutics. Lancet Oncol. 2017;18(3):e143-e52.
71. Von Hoff DD. There are no bad anticancer agents, only bad clinical trial designs--twenty-first Richard and Hinda Rosenthal Foundation Award Lecture. Clin Cancer Res. 1998;4(5):1079-86.
72. Sartore-Bianchi A, Amatu A, Bonazzina E, Stabile S, Giannetta L, Cerea G, et al. Pooled Analysis of Clinical Outcome of Patients with Chemorefractory Metastatic Colorectal Cancer Treated within Phase I/II Clinical Studies Based on Individual Biomarkers of Susceptibility: A Single-Institution Experience. Target Oncol. 2017;12(4):525-33.
73. Kovalchik S, Mietlowski W. Statistical methods for a phase II oncology trial with a growth modulation index (GMI) endpoint. Contemp Clin Trials. 2011;32(1):99-107.
74. Marcus L, Fashoyin-Aje LA, Donoghue M, Yuan M, Rodriguez L, Gallagher PS, et al. FDA Approval Summary: Pembrolizumab for the Treatment of Tumor Mutational Burden-High Solid Tumors. Clin Cancer Res. 2021;27(17):4685-9.
75. Vanpouille-Box C, Demaria S, Formenti SC, Galluzzi L. Cytosolic DNA Sensing in Organismal Tumor Control. Cancer Cell. 2018;34(3):361-78.
76. Lu C, Guan J, Lu S, Jin Q, Rousseau B, Lu T, et al. DNA Sensing in Mismatch Repair-Deficient Tumor Cells Is Essential for Anti-tumor Immunity. Cancer Cell. 2021;39(1):96-108.e6.

77. Mayer RJ, Van Cutsem E, Falcone A, Yoshino T, Garcia-Carbonero R, Mizunuma N, et al. Randomized trial of TAS-102 for refractory metastatic colorectal cancer. N Engl J Med. 2015;372(20):1909-19.
78. Grothey A, Van Cutsem E, Sobrero A, Siena S, Falcone A, Ychou M, et al. Regorafenib monotherapy for previously treated metastatic colorectal cancer (CORRECT): an international, multicentre, randomised, placebo-controlled, phase 3 trial. Lancet. 2013;381(9863):303-12.
79. Morano F, Raimondi A, Pagani F, Lonardi S, Salvatore L, Cremolini C, et al. Temozolomide Followed by Combination With Low-Dose Ipilimumab and Nivolumab in Patients With Microsatellite-Stable, O. J Clin Oncol. 2022:JCO2102583.
80. Yokota T. Are KRAS/BRAF mutations potent prognostic and/or predictive biomarkers in colorectal cancers? Anticancer Agents Med Chem. 2012;12(2):163-71.
81. Tosi F, Magni E, Amatu A, Mauri G, Bencardino K, Truini M, et al. Effect of KRAS and BRAF Mutations on Survival of Metastatic Colorectal Cancer After Liver Resection: A Systematic Review and Meta-Analysis. Clin Colorectal Cancer. 2017;16(3):e153-e63.
82. Eisenhauer EA, Therasse P, Bogaerts J, Schwartz LH, Sargent D, Ford R, et al. New response evaluation criteria in solid tumours: revised RECIST guideline (version 1.1). Eur J Cancer. 2009;45(2):228-47.
83. Li M, Chen WD, Papadopoulos N, Goodman SN, Bjerregaard NC, Laurberg S, et al. Sensitive digital quantification of DNA methylation in clinical samples. Nat Biotechnol. 2009;27(9):858-63.
84. Barault L, Amatu A, Bleeker FE, Moutinho C, Falcomatà C, Fiano V, et al. Digital PCR quantification of MGMT methylation refines prediction of clinical benefit from alkylating agents in glioblastoma and metastatic colorectal cancer. Ann Oncol. 2015;26(9):1994-9.
85. Medico E, Russo M, Picco G, Cancelliere C, Valtorta E, Corti G, et al. The molecular landscape of colorectal cancer cell lines unveils clinically actionable kinase targets. Nat Commun. 2015;6:7002.
86. Chen L, Liu P, Evans TC, Ettwiller LM. DNA damage is a pervasive cause of sequencing errors, directly confounding variant identification. Science. 2017;355(6326):752-6.
87. Taylor AM, Shih J, Ha G, Gao GF, Zhang X, Berger AC, et al. Genomic and Functional Approaches to Understanding Cancer Aneuploidy. Cancer Cell. 2018;33(4):676-89.e3.
88. Russo M, Crisafulli G, Sogari A, Reilly NM, Arena S, Lamba S, et al. Adaptive mutability of colorectal cancers in response to targeted therapies. Science. 2019;366(6472):1473-80.
89. Anagnostou V, Niknafs N, Marrone K, Bruhm DC, White JR, Naidoo J, et al. Multimodal genomic features predict outcome of immune checkpoint blockade in non-small-cell lung cancer. Nat Cancer. 2020;1(1):99-111.
90. Bergstrom EN, Huang MN, Mahto U, Barnes M, Stratton MR, Rozen SG, et al. SigProfilerMatrixGenerator: a tool for visualizing and exploring patterns of small mutational events. BMC Genomics. 2019;20(1):685.
91. Díaz-Gay M, Vila-Casadesús M, Franch-Expósito S, Hernández-Illán E, Lozano JJ, Castellví-Bel S. Mutational Signatures in Cancer (MuSiCa): a web application to implement mutational signatures analysis in cancer samples. BMC Bioinformatics. 2018;19(1):224.
92. Von Hoff DD, Stephenson JJ, Rosen P, Loesch DM, Borad MJ, Anthony S, et al. Pilot study using molecular profiling of patients' tumors to find potential targets and select treatments for their refractory cancers. J Clin Oncol. 2010;28(33):4877-83.

FIGURE

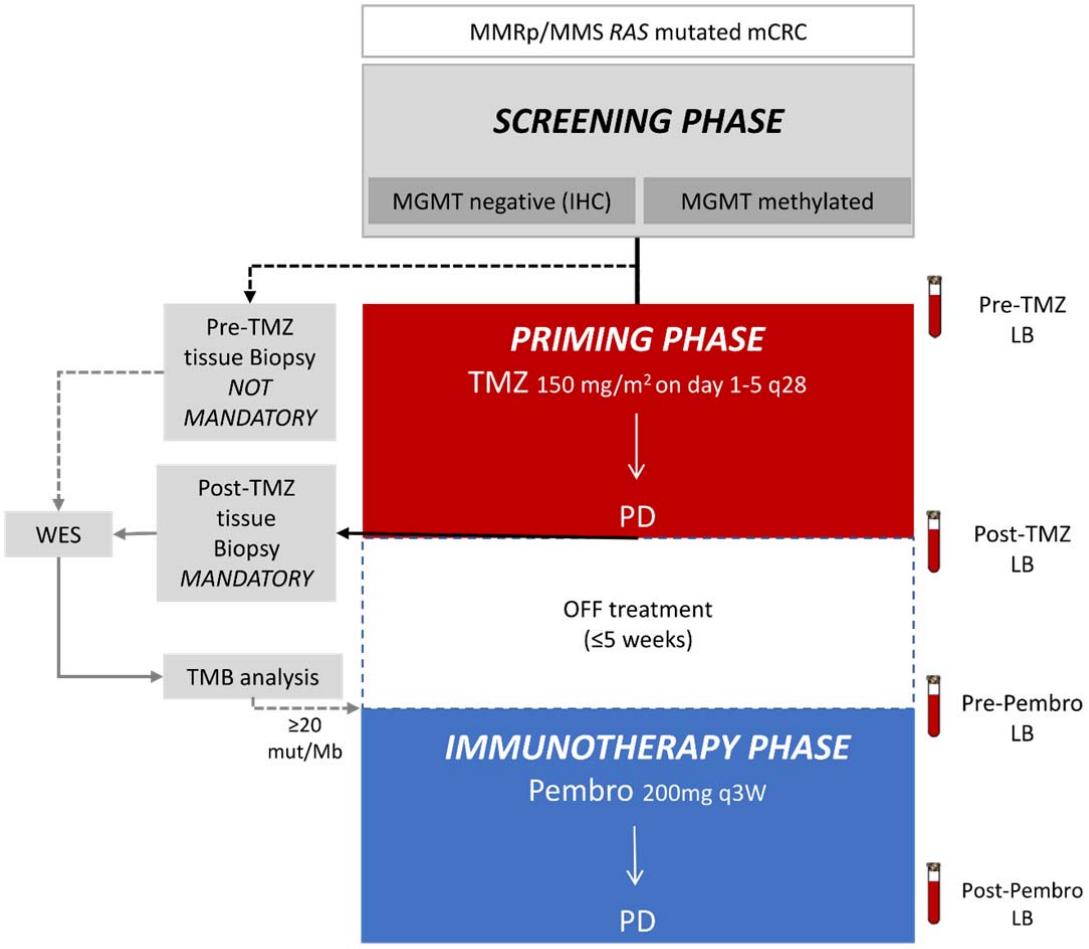

Figure 1: The ARETHUSA trial.
Graphical description of the ARETHUSA trial. (MGMT) deficient *RAS* mutant and MMR proficient mCRC patients received priming therapy with TMZ. A post-TMZ threshold of 20 mutations/Mb was required to access the *immunotherapy* phase delivering pembrolizumab every three weeks.
MMRp = mismatch repair proficient; MSS = microsatellite stable; IHC = immunohistochemistry; MB = Methyl Beaming; TMZ = temozolomide; LB = liquid biopsy; WES = Whole Exome Sequencing; TMB = Tumor Mutational Burden; PD = progressive disease; Pembro = pembrolizumab; mut = mutations; Mb = Megabases.

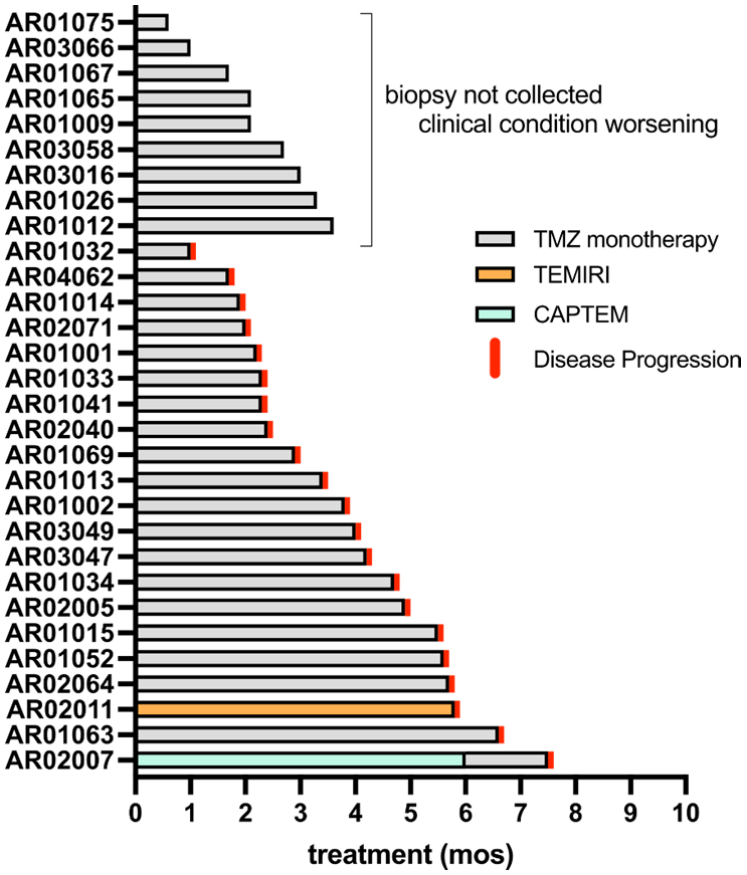

Figure 2: Clinical response to TMZ in ARETHUSA patients
Swimmer plot of clinical time on treatment in the TMZ PRIMING phase: 27 patients were treated with TMZ monotherapy until clinical or radiological (based on RECIST 1.1 criteria) disease progression. 3 Patients AR02005, AR02007 and AR02011 were treated with TMZ-based regimens and enrolled in ARETHUSA according to protocol violation. Post-TMZ tissue for TMB evaluation were collected in 21 patients, 9 cases were excluded due to clinical condition worsening. *TMZ = temozolomide; TEMIRI = TMZ + irinotecan combination; CAPTEM = capecitabine + TMZ combination; mos = months of treatment.*

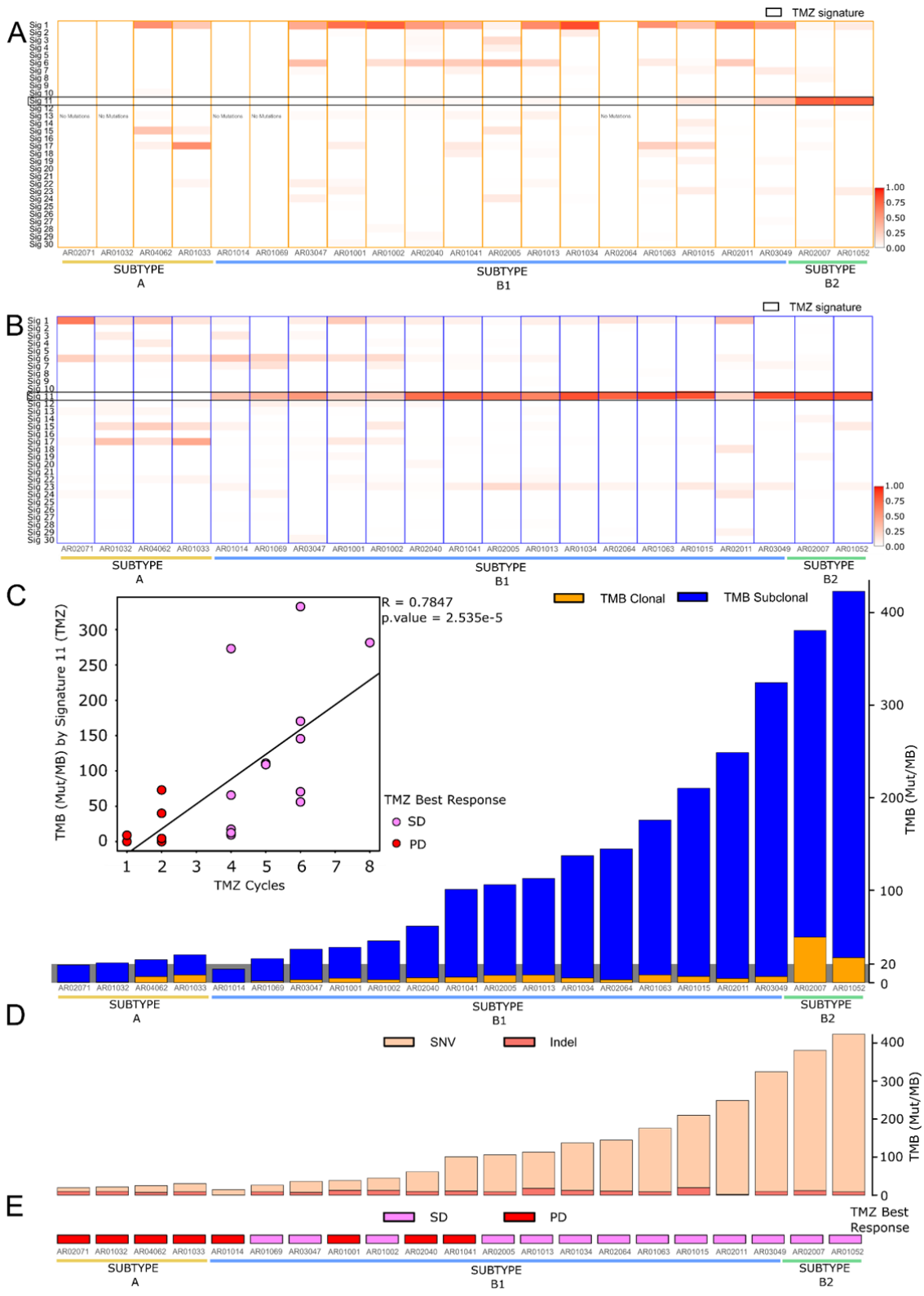
A
TMZ signature
Sig 1
Sig 2
Sig 3
Sig 4
Sig 5
Sig 6
Sig 7
Sig 8
Sig 9
Sig 10
Sig 11
Sig 12
Sig 13
Sig 14
Sig 15
Sig 16
Sig 17
Sig 18
Sig 19
Sig 20
Sig 21
Sig 22
Sig 23
Sig 24
Sig 25
Sig 26
Sig 27
Sig 28
Sig 29
Sig 30
No Mutations
1.00
0.75
0.50
0.25
0.00
AR02071 AR01032 AR04062 AR01033 AR01014 AR01069 AR03047 AR01001 AR01002 AR02040 AR01041 AR02005 AR01013 AR01034 AR02064 AR01063 AR01015 AR02011 AR03049 AR02007 AR01052
SUBTYPE A
SUBTYPE B1
SUBTYPE B2
B
TMZ signature
C
R = 0.7847
p.value = 2.535e-5
TMB (Mut/MB) by Signature 11 (TMZ)
TMZ Cycles
TMZ Best Response
SD
PD
TMB Clonal
TMB Subclonal
TMB (Mut/MB)
D
SNV
Indel
E
SD
PD
TMZ Best Response

Figure 3: Mutational signature and TMB analysis in biopsies after TMZ treatment.

A-B): Mutational signature analysis measuring the impact of TMZ priming on tissue biopsies assessed by NGS. Patients were classified in three subtypes A, B1 and B2 based on the score of the mutational signature 11 and TMB value. In panel **A**, only clonal mutations (adjusted fractional abundance $\geq$ 10%) were used to generate the heatmap. In five cases (AR02071, AR01032, AR01014, AR01069 and AR02064) the number of mutations was not sufficient to properly perform mutational analysis (cosine similarity lower than 0.9) and these five samples were excluded. In panel **B**, all mutations (adjusted fractional abundance $\geq$ 1%) were considered for heatmap generation. **C):** TMB expressed as mut/MB after the priming phase for the three groups of patients. The relative contribution of clonal (yellow) and subclonal (blue) alterations to TMB is listed for each patient. **Inset panel C:** Positive linear correlation between mutations induced by Signature 11 (TMZ) normalized for megabases and temozolomide cycles of treatment. Spearman's rank correlation is listed (p-value = 2.535e-5 and Cor = 0.7847). **D)** TMB expressed as mutations/megabases after the priming phase for the three groups of patients. The relative contribution of SNVs and INDELs to TMB is listed for each patient**. E)** The best response to TMZ treatment is also reported for each patient. *SUBTYPE A (yellow): patients with no molecular evidence of TMZ treatment. SUBTYPE B1 (blue): patients with subclonal molecular evidence of TMZ treatment. SUBTYPE B2 (green): patients with clonal molecular evidence of TMZ treatment. TMZ= temozolomide; TMB= Tumor Mutational Burden; Mut/MB = mutations for megabases. Sig= Signature, SNV = single nucleotide variant; INDEL = insertions and deletions; SD = Stable disease; PD = progressive disease.*

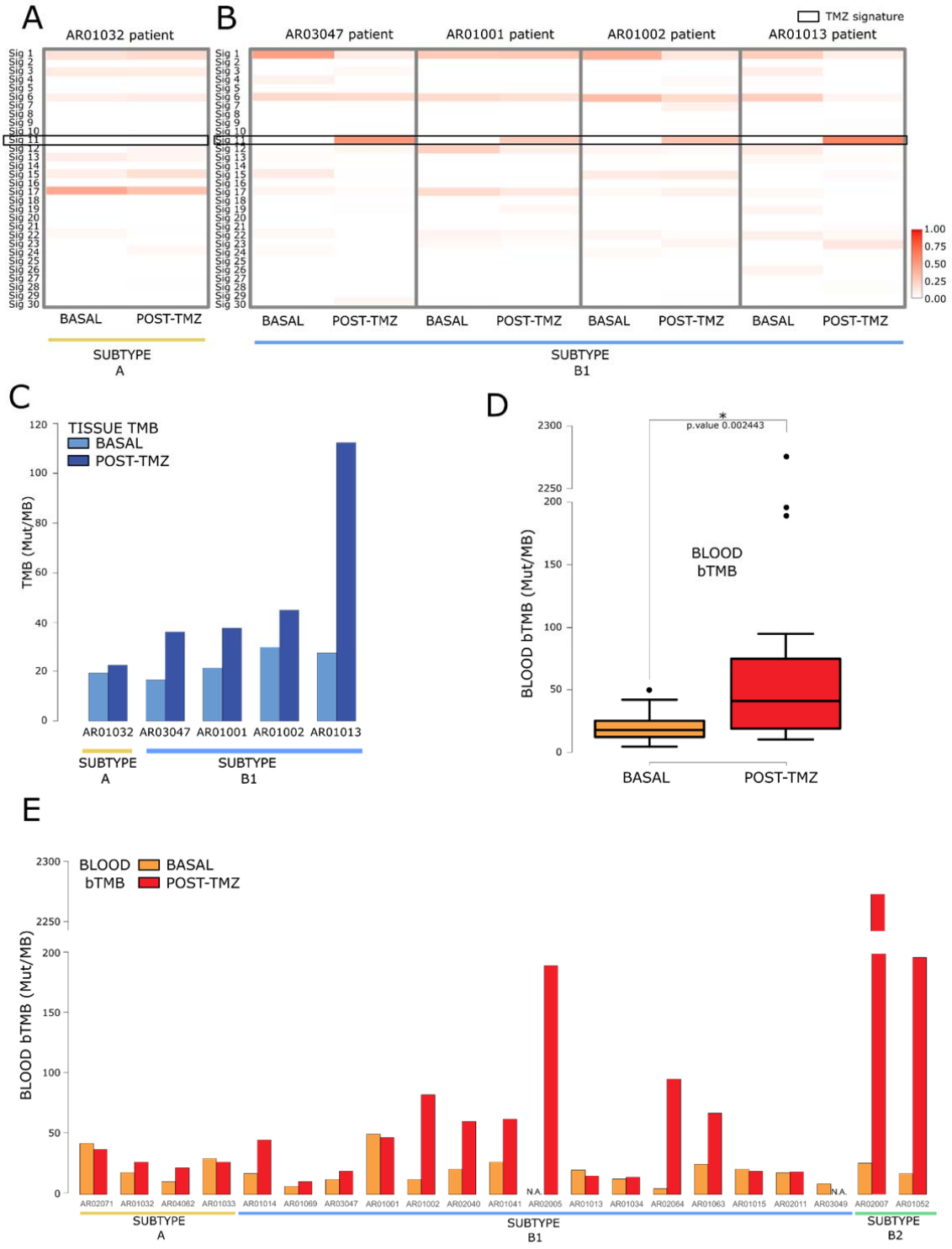

Figure 4: Comparison of signature and TMB analysis of tissue/blood samples before and after TMZ priming

A): Signature contribution before and after TMZ priming in tissue sample of subtype A patients; **B):** Signature contribution before and after TMZ priming in tissue samples

of the subtype B patients; **C):** TMB in tumor tissue before and after TMZ priming; **D-E):** Blood Tumor Mutational Burden (bTMB) expressed as Mut/MB before and after the TMZ priming phase in aggregate **(D)** and in detail for each patient **(E).** Wilcoxon rank sum test, p.value = 0.002443. *Subtype A: patients with no genetic evidence of Temozolomide treatment. Subtype B1: patients with subclonal genetic evidence of Temozolomide treatment; Subtype B2: patients with clonal genetic evidence of Temozolomide treatment; TMZ= temozolomide; TMB= Tumor Mutational Burden; Mut/MB = mutations for megabases; Sig= Signature; BASAL= analysis of tumor before Priming Phase of ARETHUSA trial; Post-TMZ= analysis of tumor after Priming Phase of ARETHUSA trial. N.A. = Not Available*

A

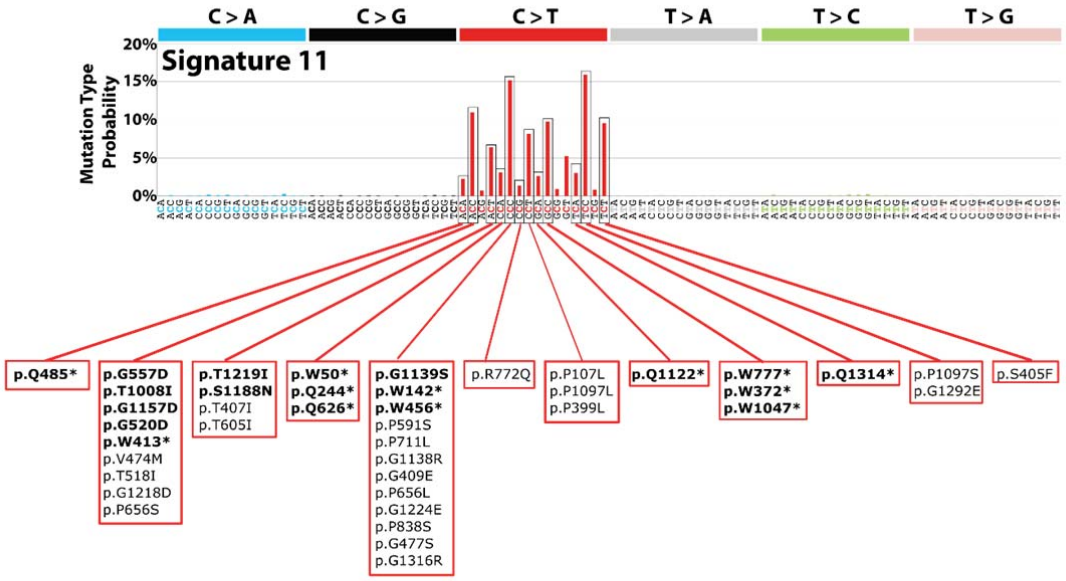

B

MSH6 alteration	coord	Patient	Patient_ID	dMMR status
p.T1219I	chr2:48033352	15	AR01014; AR01001; AR01002; AR02005; AR010013; AR01015; AR01034; AR01041; AR02040; AR02011; AR02007; AR03049; AR01052; AR01063; AR02064	Drost et al., 2020
p.G557D	chr2:48026792	2	AR01034; AR02005	Drost et al., 2020
p.T1008I	chr2:48028145	2	AR02005; AR01052	Drost et al., 2020
p.Q1122*	chr2:48030750	2	AR02007; AR02064	STOP codon acquisition
p.W777*	chr2:48027453	1	AR01034	STOP codon acquisition
p.W50*	chr2:48010521	1	AR01034	STOP codon acquisition
p.G1139S	chr2:48030801	1	AR02007	Drost et al., 2020
p.W142*	chr2:48018231	1	AR02007	STOP codon acquisition
p.Q1314*	chr2:48033729	1	AR02007	STOP codon acquisition
p.W372*	chr2:48026238	1	AR02007	STOP codon acquisition
p.Q244*	chr2:48025852	1	AR02007	STOP codon acquisition
p.G1157D	chr2:48032080	1	AR02005	Drost et al., 2020
p.G520D	chr2:48026681	1	AR02005	Drost et al., 2020
p.W413*	chr2:48026361	1	AR02005	STOP codon acquisition
p.W456*	chr2:48026490	1	AR02005	STOP codon acquisition
p.Q626*	chr2:48026998	1	AR02005	STOP codon acquisition
p.W1047*	chr2:48028263	1	AR01063	STOP codon acquisition
p.S1188N	chr2:48032763	1	AR01063	Drost et al., 2020
p.Q485*	chr2:48026575	1	AR01063	STOP codon acquisition
p.K301fs*12	chr2:48026024	1	AR01069	STOP codon acquisition
p.G409E	chr2:48026348	2	AR02040; AR01063	
p.P591S	chr2:48026893	1	AR02005	
p.P107L	chr2:48018125	1	AR02005	
p.P711L	chr2:48027254	1	AR02005	
p.P1097S	chr2:48030675	1	AR02005	
p.V474M	chr2:48026542	1	AR01013	
p.P1097L	chr2:48030676	1	AR01015	
p.G1292E	chr2:48033664	1	AR01015	
p.R772Q	chr2:48027437	1	AR01015	
p.G1138R	chr2:48030798	1	AR01034	
p.S405F	chr2:48026336	1	AR02040	
p.P656L	chr2:48027089	1	AR02011	
p.P656S	chr2:48027088	1	AR02064	
p.P399L	chr2:48026318	1	AR02064	
p.P838S	chr2:48027634	1	AR01063	
p.T518I	chr2:48026675	1	AR01063	
p.G477S	chr2:48026551	1	AR01063	
p.G1218D	chr2:48033349	1	AR01063	
p.G1316R	chr2:48033735	1	AR01063	
p.T407I	chr2:48026342	1	AR02007	
p.G1224E	chr2:48033367	1	AR02007	
p.T605I	chr2:48026936	1	AR02007	

Figure 5: *MSH6* genetic alterations in ARETHUSA patients and their genetic context

A): Mutation type probability according to Signature 11 and *MSH6* mutations emerged after TMZ treatment. The contexts of each mutation in *MSH6* gene in both

tissue biopsy and blood post-TMZ priming were shown; mutations which are likely to inactivate MMR are reported in bold. **B):** *MSH6* genetic alterations identified in tissue and blood after TMZ priming. Mutations potentially affecting the MMR status (MMRp to MMRd) are listed in bold. *dMMR =deficient Mismatch Repair*

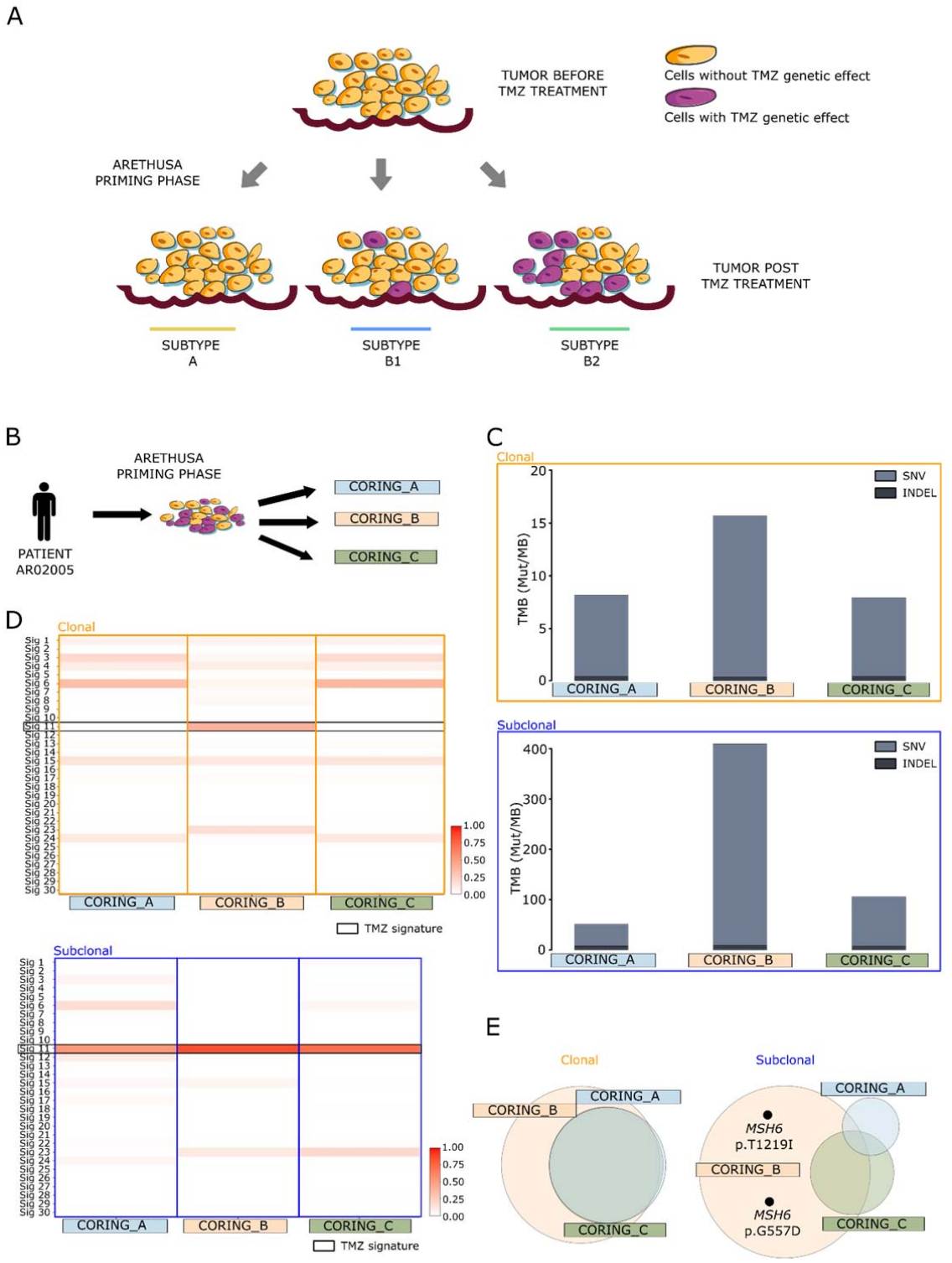

Figure 6. Molecular intra-lesion heterogeneity was induced by TMZ, affecting distinct regions of the same lesion at different manner.

A): Scheme of proposal tumor response to TMZ treatment, the percentage of cell showing TMZ genetic effect was different in three different tumor subtypes. **B):** scheme of the experiment. **C):** TMB in the three corings with relative contribution of SNV/Indel was reported at clonal (upper) and subclonal level (below). **D)**: Signature analysis at clonal (upper) and subclonal level (below) of three corings **E):** Venn diagram of common, shared and private genetic alterations in the three corings at clonal (left) and subclonal (right) level. Variants *MSH6* p.T1219I and p.G557D were shown in the private mutations of subclonal coring B. *TMZ= temozolomide; TMB= Tumor Mutational Burden; Mut/MB = mutations for megabases; Sig= signature; SNV = single nucleotide variant; INDEL = insertions and deletions*

Fig 7

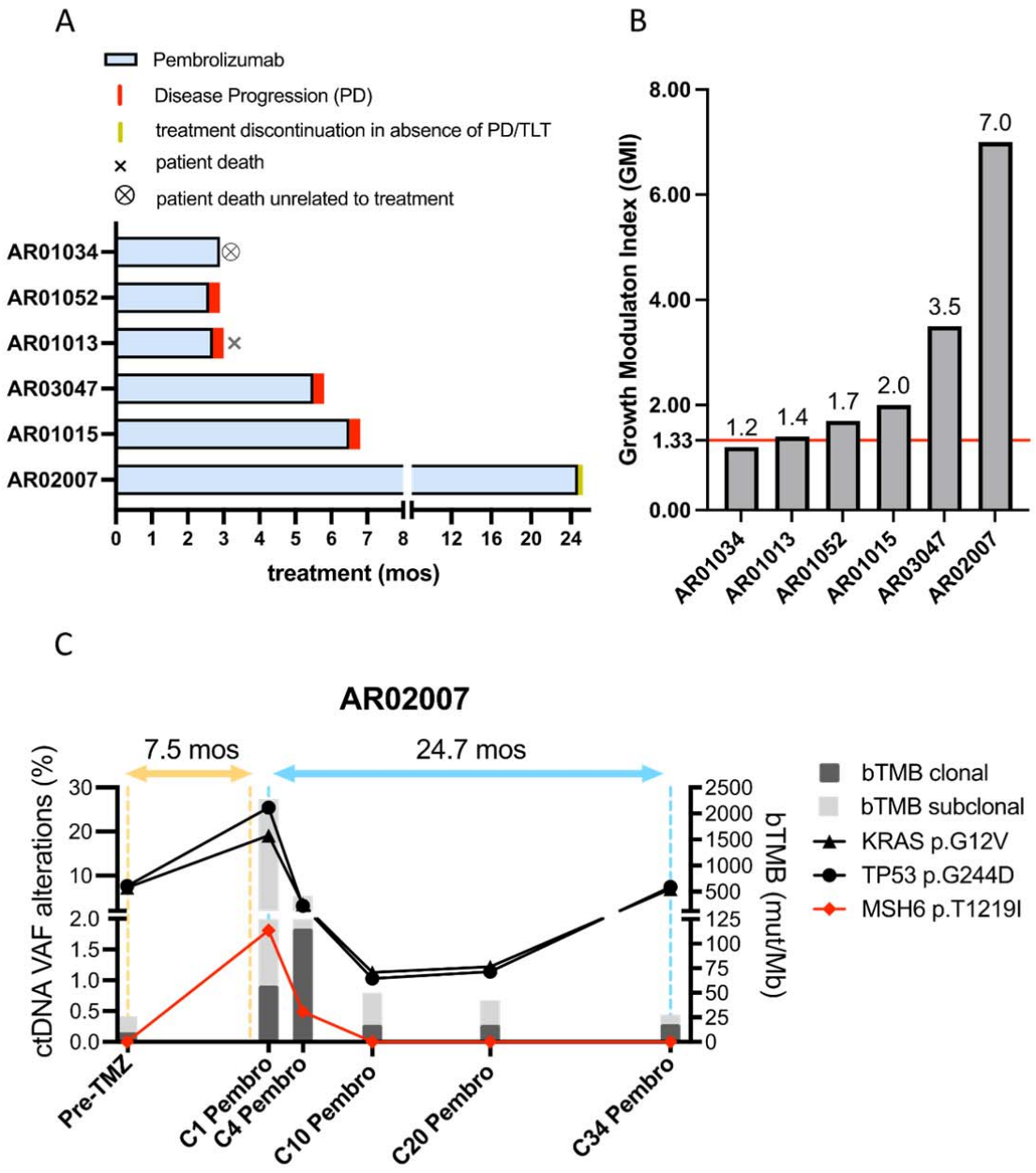

Figure 7: Clinical impact of pembrolizumab on MMRp mCRC patients after TMZ priming

A): Swimmer plot of 6 patients that achieved high TMB after TMZ priming and were treated with pembrolizumab monotherapy until progression; two patients had progressive disease after 3 and 4 cycles, while three patients were treated for 7, 9 and 33 cycles with long-lasting disease stabilization before progression. 1 patient died for unrelated cause with tumor stabilization after 5 cycles. **B):** Growth modulation index (GMI) for each patient primed with TMZ and treated with Pembrolizumab. Red bar indicates the cut-off of 1.33 considered as clinically meaningful. **C)** Graph shows longitudinal, liquid biopsy-based ctDNA monitoring of the patient AR02007 during priming (TMZ-based therapy) and immunotherapy

(pembrolizumab) phases of ARETHUSA. Colored lines indicate clonal evolution of trunk/driver mutations (*KRAS* and *TP53*; black) and *MSH6* p.T1219I variant (red) detected by ctDNA analysis at the indicated time-points. TMB in blood (clonal and subclonal bTMB) at each time-point is also reported (dark and light gray bar). *mos = months of treatment; bTMB = blood Tumor Mutational Burden; ctDNA = circulating tumor DNA; TMZ-based = Temozolomide-based treatment; VAF = Variant Allele Frequency; TLT = Treatment Limiting Toxicity*

TABLES

Genetic TMZ effect	Patient_ID	TMZ_Signature (score)	MSH6 alterations (post TMZ) in tissue	MSH6 alterations (pre TMZ) in blood	MSH6 alterations (post TMZ) in blood
SUBTYPE A: no genetic TMZ effect	**AR02071**	**0**	-	-	-
SUBTYPE A: no genetic TMZ effect	**AR01032**	**0**	-	-	-
SUBTYPE A: no genetic TMZ effect	**AR04062**	**0**	-	-	-
SUBTYPE A: no genetic TMZ effect	**AR01033**	**0**	-	-	-
SUBTYPE B1: subclonal effect	**AR01014**	**0,31**	-	-	p.T1219I
SUBTYPE B1: subclonal effect	**AR01069**	**0,39**	p.K301fs*12	-	-
SUBTYPE B1: subclonal effect	**AR03047**	**0,53**	-	-	p.T1219I[1]
SUBTYPE B1: subclonal effect	**AR01001**	**0,27**	-	-	p.T1219I
SUBTYPE B1: subclonal effect	**AR01002**	**0,30**	-	-	p.T1219I
SUBTYPE B1: subclonal effect	**AR02040**	**0,72**	-	-	p.T1219I
SUBTYPE B1: subclonal effect	**AR01041**	**0,77**	-	-	p.T1219I
SUBTYPE B1: subclonal effect	**AR02005**	**0,72**	p.T1219I;p.G557D	NA	p.T1219I;p.G557D; p.Q626*; p.W456*; p.W413*; p.G520D; p.G1157D; p.T1008I
SUBTYPE B1: subclonal effect	**AR01013**	**0,63**	-	-	p.T1219I
SUBTYPE B1: subclonal effect	**AR01034**	**0,84**	p.T1219I;p.G557D; p.V777*; p.W50*	-	p.T1219I
SUBTYPE B1: subclonal effect	**AR02064**	**0,77**	-	-	Q1122*; p.T1219I
SUBTYPE B1: subclonal effect	**AR01063**	**0,87**	p.W1047*	-	p.T1219I;p.S1188N; p.Q485*
SUBTYPE B1: subclonal effect	**AR01015**	**0,84**	p.T1219I	-	p.T1219I
SUBTYPE B1: subclonal effect	**AR02011**	**0,23**	p.T1219I	-	p.T1219I
SUBTYPE B1: subclonal effect	**AR03049**	**0,86**	p.T1219I	-	NA
SUBTYPE B2: clonal effect	**AR02007**	**0,85**	p.G1139S	-	p.G1139S; p.T1219I; p.Q1122*; p.W142*; p.Q1314*; p.W372*; p.Q244*
SUBTYPE B2: clonal effect	**AR01052**	**0,84**	-	-	p.T1219I;p.T1008I

Table 1: Molecular features of ARETHUSA patients
For each patient, the molecular effect of TMZ, the relative contribution of Signature 11 in tissue samples after TMZ and occurrence of *MSH6* mutations identified in the blood (red color) before and after the TMZ treatment are listed. Variants of unknown significance were filtered and only mutations likely to inactivate MMR system are listed. *Sig.=Signature; TMZ = Temozolomide; Subtype A= patients with no molecular evidence of Temozolomide treatment. Subtype B1= patients with subclonal molecular evidence of Temozolomide treatment. Subtype B2= patients with clonal molecular evidence of Temozolomide treatment. NA = Not Available. [1]identified during Pembrolizumab longitudinal monitoring (at cycle 7).*

Supplementary Information and description

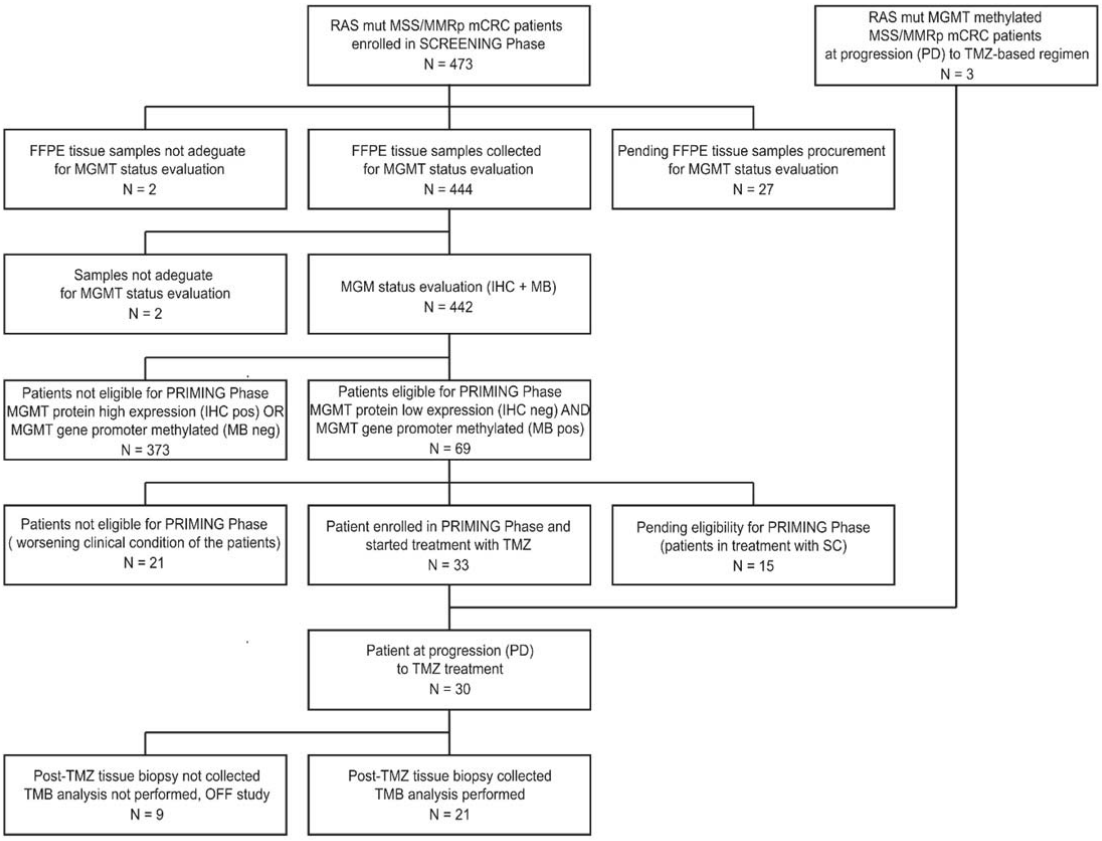

Supplementary Figure S1:

CONSORT diagram of patients screened for the ARETHUSA trial (N=473), and eligible for the temozolomide PRIMING (N=69) and evaluated according to IMMUNOTHERAPY eligibility criteria (N = 30) as described in this study. *N = Numbers; TMZ = Temozolomide; PD=progressive disease; MSS = microsatellite stable; MMRp = mismatch repair proficient; mut = mutant; FFPE = Formalin-Fixed Paraffin-Embedded; mCRC = metastatic Colorectal cancer; IHC=immunohistochemistry; MB=methyl beaming; pos = positive; neg = negative; TMB = Tumor Mutational Burden; SC =Standard Care; O6-Methylguanine-DNA-methyltransferase (MGMT).*

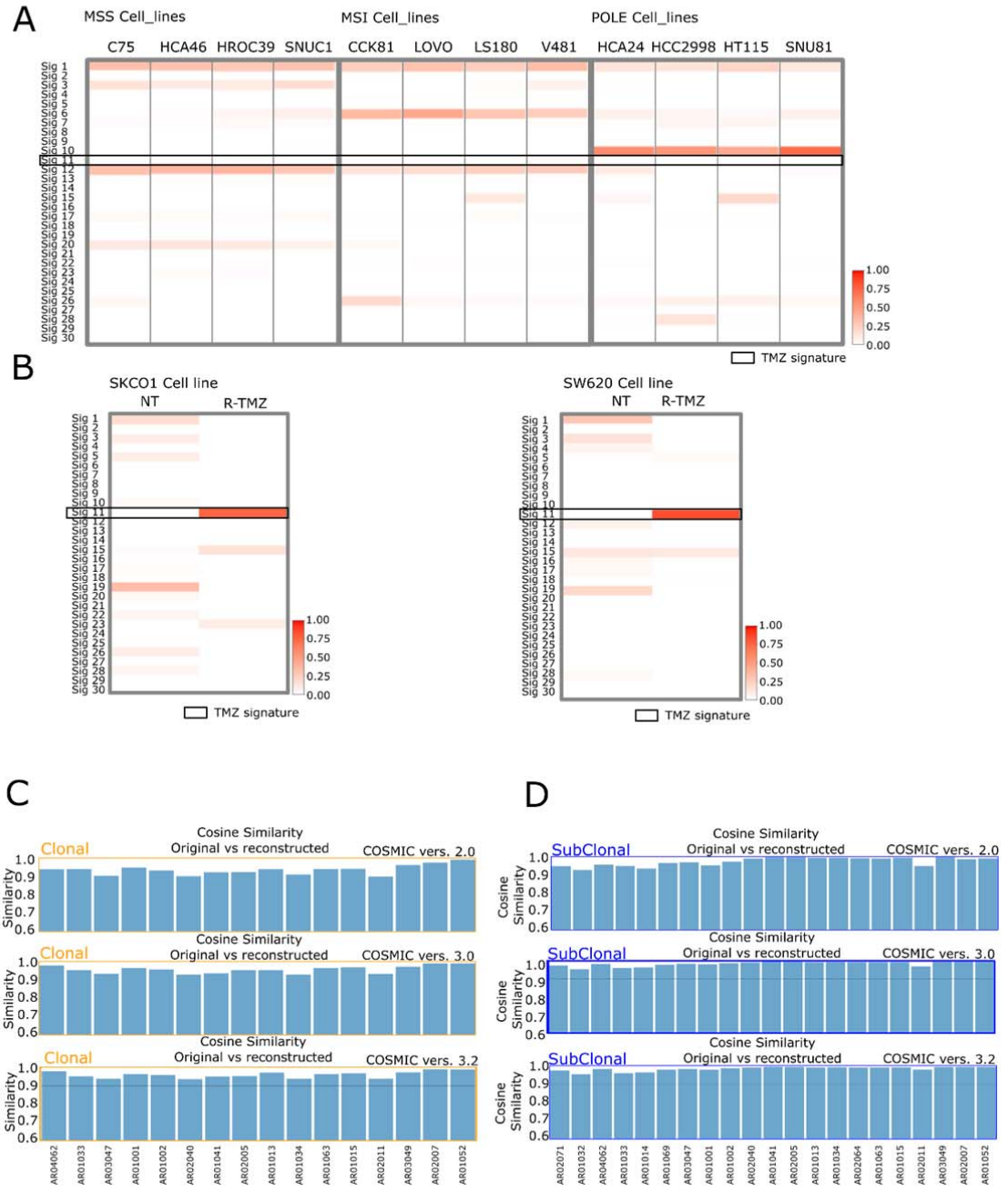

Supplementary Figure S2:
A) Profile of mutational signatures in a panel of 12 CRC cell lines according to the indicated genetic features. **B)** Profile of mutational signatures in parental SKCO1 and SW620 cell lines and in their R-TMZ resistant counterparts**. C-D)** Comparison of cosine similarity calculated between original vs reconstructed mutational profiles of tissues post TMZ. Three different reference databases were used: COSMIC version 2.0 (top), COSMIC vers 3.0 (center) and COSMIC vers 3.2 (bottom) **C)** Analysis was performed using only clonal mutations (fractional abundance ≥ 10%). In five cases (AR02071, AR01032, AR01014, AR01069 and AR02064) the cosine similarity was

lower than 0.9. **D)** Analysis was performed using both clonal and subclonal mutations (fractional abundance ≥ 1%). *vers. = version; TMZ= Temozolomide; NT= not treated; R-TMZ= resistant to TMZ; Sig= Signature; MSS=microsatellite stable; MSI= microsatellite instable; DNA polymerase epsilon (POLE) mutations*.

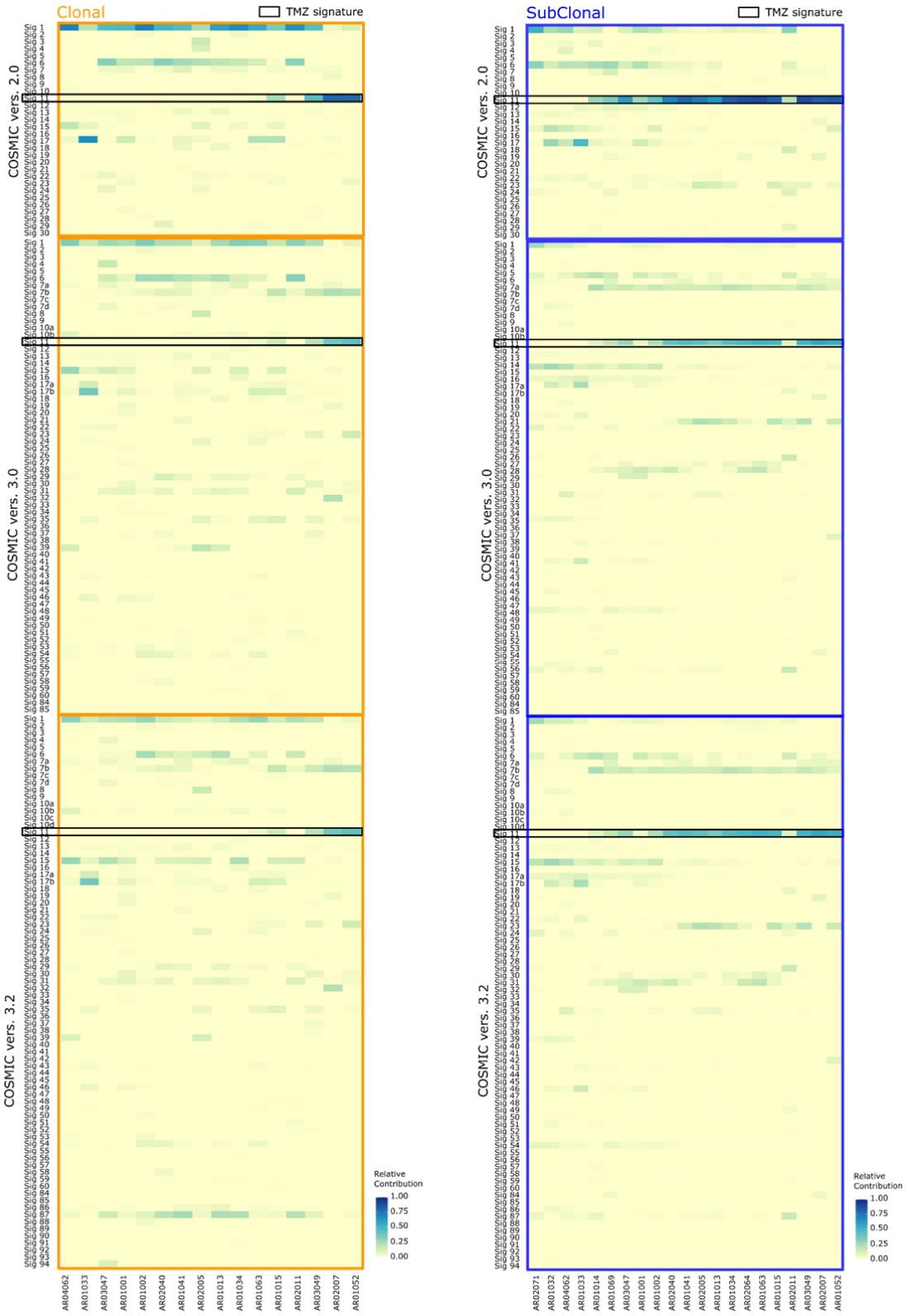

Supplementary Figure S3:

Mutational signatures in tumor biopsies obtained after TMZ priming

A) Signature contribution analysis considering clonal mutations (fractional abundance ≥ 10%) for the heatmap generation and considering three different Signature reference databases (COSMIC ver. 2.0, ver. 3.0 and ver. 3.2). In five cases (AR02071, AR01032, AR01014, AR01069 and AR02064) the number of mutations was not sufficient to properly perform mutational analysis (cosine similarity lower than 0.9) and these five samples were excluded. **B)** Signature contribution analysis considering clonal and subclonal mutations (fractional abundance ≥ 1) for the heatmap generation, using three different signatures reference databases (COSMIC ver. 2.0, ver. 3.0 and ver. 3.2). Signature 11 related to alkylating agent was highlighted. *Sig.=Signature; TMZ = Temozolomide; vers. = version.*

Fig S4

A

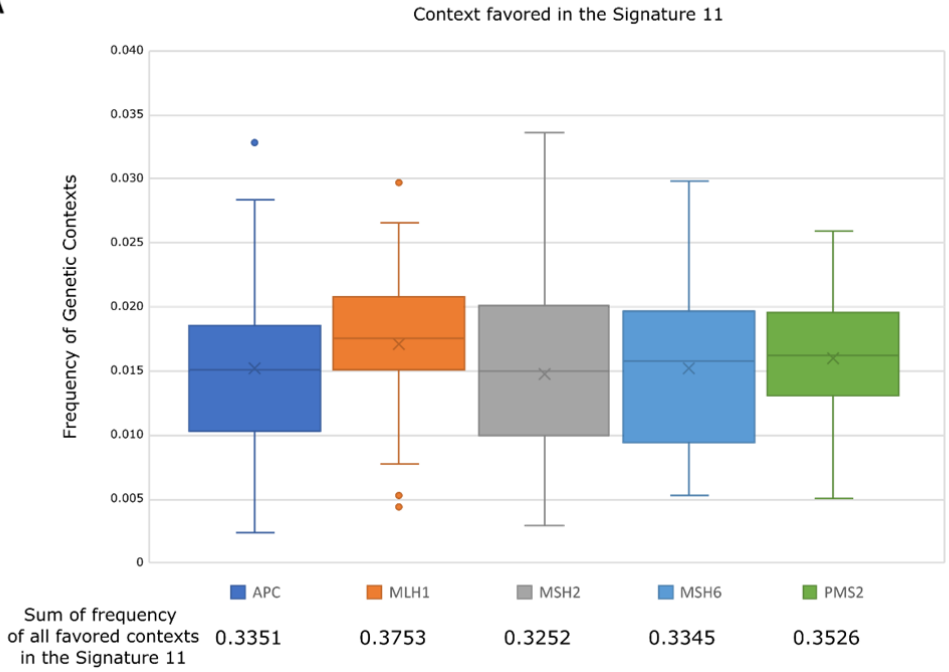

B

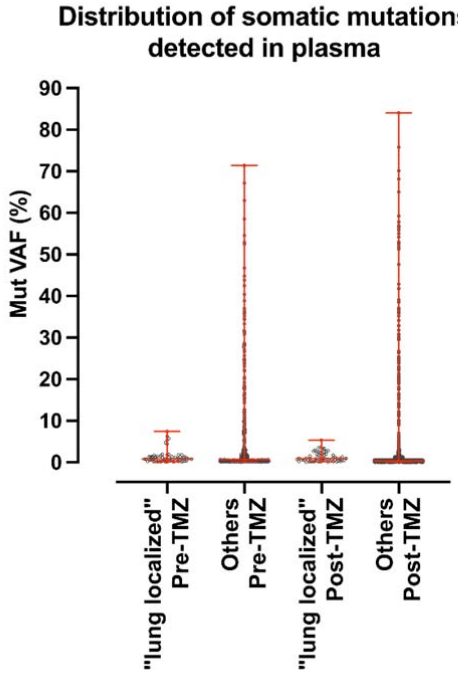

	"lung localized" Pre-TMZ	Others Pre-TMZ	"lung localized" Post-TMZ	Others Post-TMZ
Number of values	60	393	62	3531
Minimum	0.1400	0.06000	0.1000	0.01000
25% Percentile	0.3400	0.2900	0.3725	0.2300
Median	0.8550	0.6800	0.9250	0.3400
75% Percentile	1.400	6.765	1.988	0.6300
Maximum	7.420	71.42	5.350	84.04
Range	7.280	71.36	5.250	84.03

Supplementary Figure S4:

A) Frequency of alterations in the nucleotide context modified by TMZ signature 11 compared to all nucleotide contexts for *APC* and the MMR genes. Sum of frequency

of all favored contexts in the Signature 11 were reported (Methods for details). **B)** Distribution of the somatic mutations identified in plasma collected before and after the TMZ treatment in patients with lesions exclusively localized in lung ("Lung localized") and in patients with lesions localized also or only in liver ("Others"). *Mut = Mutation; VAF = Variant Allelic Frequency; TMZ = Temozolomide; X is the average value*

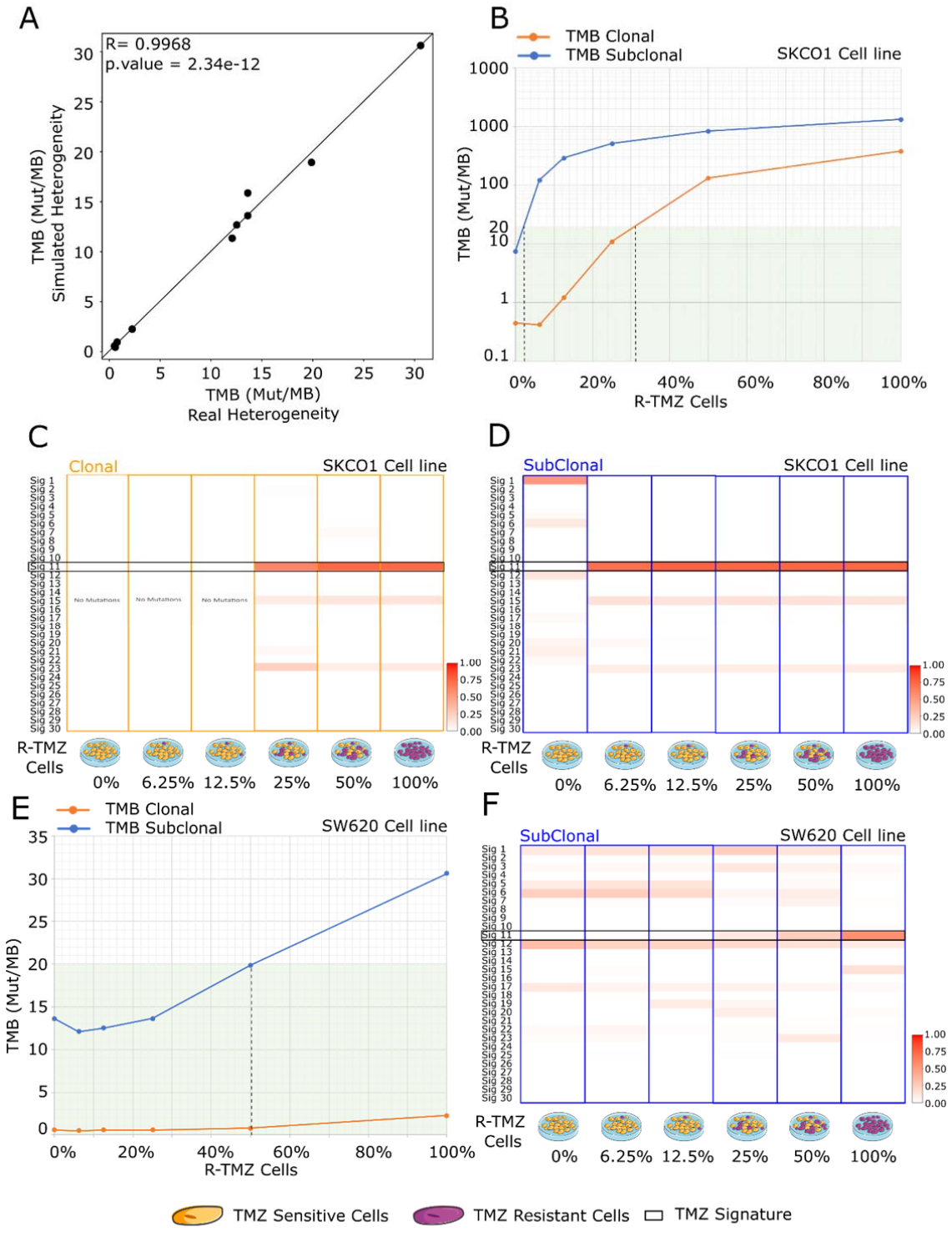

Supplementary Figure S5:

Impact of molecular heterogeneity on mutational signatures and TMB in CRC cell lines treated according to a TMZ schedule which parallels ARETHUSA therapy. **A):**

Positive Linear Correlation between TMB calculated using real and simulated data, Pearson's product-moment correlation is reported (R = 0.9968) with p-value = 2.34e-12. **B)** Increase of TMB observed by extending the fractional abundance of the TMZ resistant SKCO1 cells **C-D):** Effect of the heterogeneity on the Signature 11. By increasing the fractional abundance of TMZ resistant cells the contribution of signature 11 increased. The signature contribution was calculated considering only clonal mutation in panel **C** and considering all genetic alteration in panel **D** for the SKCO1 cell line. **E):** Effect of heterogeneity on TMB. Increase of Tumor Mutational Burden enlarging the fractional abundance of the TMZ resistant cells in SW620 cell line**. F):** Effect of the heterogeneity on the Signature 11 (related to Temozolomide). By increasing the fractional abundance of TMZ resistant cells the contribution of signature 11 increased. The signature contribution was calculated considering all genetic alteration for the SW620 cell line. *Sig.=Signature; TMZ = Temozolomide; TMB= Tumor Mutational Burden; R-TMZ= resistant to temozolomide treatment; Mut/MB = Mutations for megabases*

Fig S6

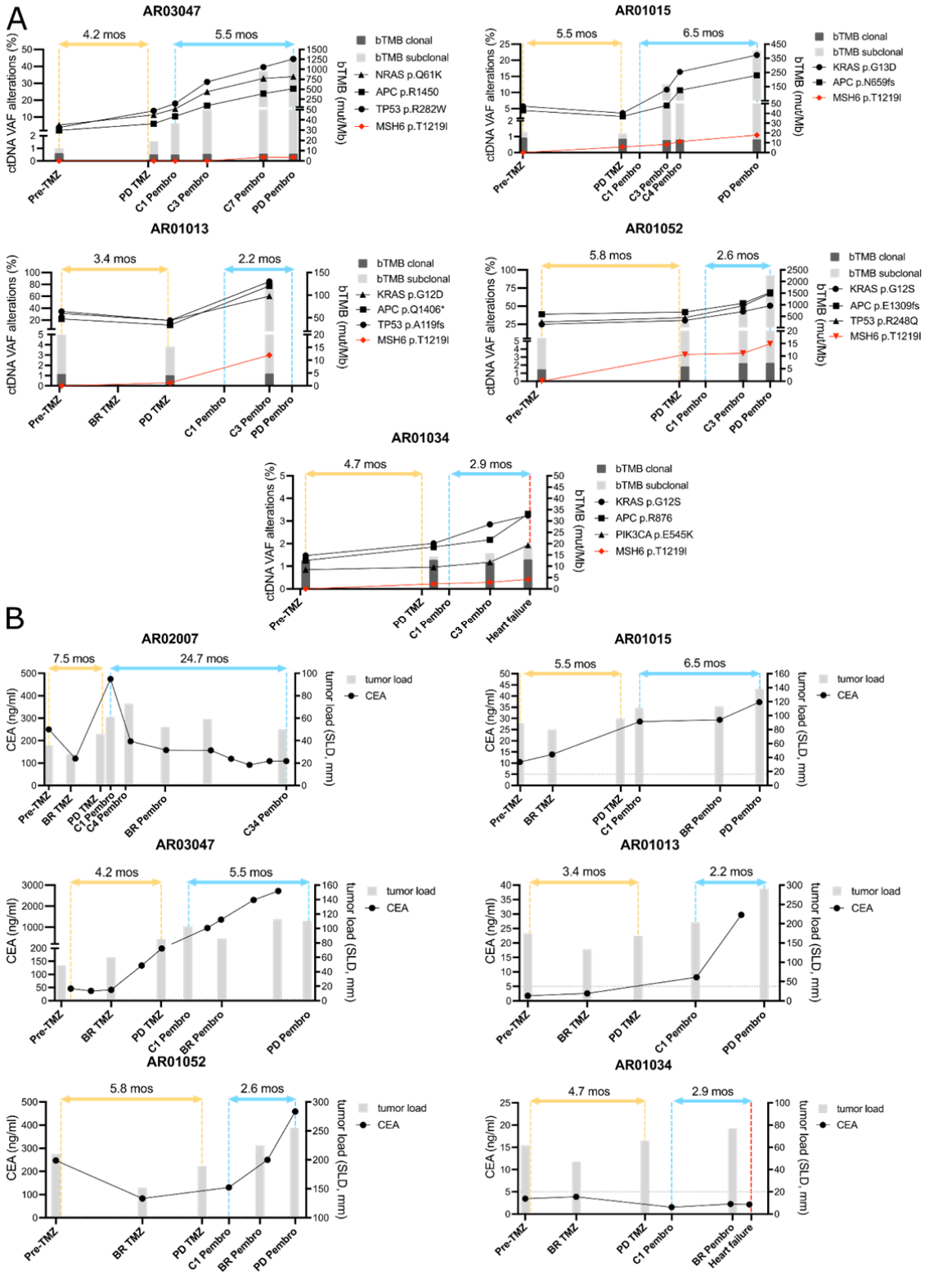

Supplementary Figure 6

A: Graphs show longitudinal, liquid biopsy-based ctDNA monitoring of the patients AR03047, AR01015, AR01013, AR01052 and AR01034 during TMZ priming and immunotherapy. Colored lines indicate clonal evolution of trunk/driver mutations. *KRAS, TP53; APC; NRAS PIK3CA* are shown in black and *MSH6* p.T1219I variant is in red. bTMB (clonal and subclonal) at each time-point is also reported (dark and light gray bar). **B:** Longitudinal monitoring of CEA levels (ng/ml) and tumor load (SLD, mm) in patients during TMZ and pembrolizumab treatment. Mo= Months. ORR = Objective Response Rate; SD= Stable Disease; PD=Progression Disease.

Clinical feature		Evaluated Patients (n=21)	
Age (median, range)		62	28-84
Gender (n; %)	M	10	47,6
	F	11	52,4
Primary T location (n; %)	Rectum	4	19,0
	Colon	17	81,0
Sidedness (n; %)	Left	14	66,7
	Right	7	33,3
MSS/MMR status (n; %)	MMS/MMRp	21	100,0
MGMT status (median, range)	ICH score	15	(0-75)
	MB score	78,0%	(41,2-100,0)
RAS mutation (n; %)	G12	13	61,9
	G13	4	19,0
	other	4	19,0
Baseline Metastasis localization (n; %)	thoracic only	2	9,5
	abdomen only	0	0,0
	liver only	0	0,0
	liver+abdomen	3	14,3
	liver+lung	6	28,6
	diffuse	10	47,6

Sample_ID	READS	Depth (X)	Coverage 1X (%)	Coverage 10X (%)	Coverage 100X (%)
AR01001_NORMAL	137970480	398	97,93	97,60	96,74
AR01001_postTMZ	152192214	419	97,95	97,63	96,92
AR01001_preTMZ	104877109	308	97,87	97,54	96,04
AR01002_NORMAL	106327402	315	97,99	97,64	96,19
AR01002_postTMZ	112052167	327	98,02	97,69	96,15
AR01002_preTMZ	159382962	448	98,04	97,71	97,02
AR01013_NORMAL	102499935	307	98,05	97,69	95,57
AR01013_postTMZ	131734771	376	98,06	97,68	95,77
AR01013_preTMZ	120746214	236	97,96	97,54	91,88
AR01014_NORMAL	157500667	414	97,83	97,48	96,21
AR01014_postTMZ	133532979	368	97,83	97,46	95,79
AR01015_NORMAL	92516393	288	97,88	97,51	95,94
AR01015_postTMZ	96139405	298	97,89	97,52	96,16
AR01032_NORMAL	156046824	425	98,03	97,70	96,82
AR01032_postTMZ	149247970	445	98,02	97,68	96,94
AR01032_preTMZ	77448370	240	97,92	97,57	96,82
AR01033_NORMAL	158543286	442	98,10	97,74	96,96
AR01033_postTMZ	142797558	383	98,01	97,67	96,60
AR01034_NORMAL	118705353	341	98,03	97,67	96,42
AR01034_postTMZ	154048005	435	98,04	97,68	96,91
AR01041_NORMAL	109343403	376	98,47	98,06	97,11

AR01041_postTMZ	74171029	259	98,38	97,94	95,91
AR02005_NORMAL	127530660	370	97,90	97,57	96,69
AR02005_postTMZ_1	121508468	363	97,85	97,50	96,32
AR02005_postTMZ_2	127373174	372	97,84	97,49	96,08
AR02005_postTMZ_3	94134643	272	97,84	97,48	95,08
AR02007_NORMAL	95334938	291	97,82	97,46	95,84
AR02007_postTMZ	110226608	332	97,85	97,49	96,16
AR02011_NORMAL	182153134	503	98,07	97,75	97,05
AR02011_postTMZ	87167583	202	97,64	97,19	91,47
AR02040_NORMAL	128296851	432	98,53	98,11	97,31
AR02040_postTMZ	110294428	359	98,50	98,08	97,02
AR03047_NORMAL	123322335	414	98,59	98,21	97,32
AR03047_postTMZ	88348171	302	98,51	98,13	96,63
AR03049_NORMAL	111500850	364	98,68	98,24	97,08
AR03049_postTMZ	145085723	444	98,72	98,30	97,28
AR03049_preTMZ	136694718	433	98,65	98,25	97,29
AR01052_NORMAL	193787690	499	98,40	98,02	97,15
AR01052_postTMZ	183422134	457	98,33	97,94	96,83
AR04062_postTMZ	110640087	349	98,50	98,09	96,68
AR04062_NORMAL	132059504	417	98,56	98,16	97,16
AR01069_postTMZ	124020946	365	98,65	98,24	96,82
AR01069_NORMAL	140021771	412	98,66	98,27	97,14
AR02064_NORMAL	136445500	432	98,69	98,28	97,16
AR02064_postTMZ	122566050	395	98,58	98,18	97,08
AR01063_NORMAL	156283925	490	98,63	98,22	97,31
AR01063_postTMZ	110074395	346	98,50	98,08	96,75
AR02071_postTMZ	120976134	385	98,71	98,31	97,32
AR02071_NORMAL	130673258	420	98,72	98,33	97,45

Supplementary Table S1:

Sheet1: Main clinicopathological features of patients enrolled in the ARETHUSA trial between April 2019 and December 2021 who underwent tissue biopsy following progressive disease after TMZ priming. *MMRp=mismatch repair proficient; MSS=microsatellite stable; MGMT= O[6]-methylguanine-DNA methyltransferase ; IHC=immunohistochemistry; MB=methyl beaming; n = number; TMB=Tumor Mutational Burden; PD=progressive disease; mut=mutant; N.A = not available; M = male; F = female;*

Sheet2: Summary of the NGS parameters of tissue samples. The numbers of sequenced reads, median Depth (X) and median coverage at median 1X and 10X and 100X depth are reported for each sample. *preTMZ= before temozolomide treatment, postTMZ= after temozolomide treatment;*

Patient ID	Age	Gender	Primary T localization	*RAS* mutation	Subtype	Signature TMZ (subclonal, Score)	TMB (subclonal, Mut/MB)	TMZ Priming		bTMB (Mut/MB)		*RAS* extended mut		Lesions localization (new lesions post-TMZ)				
								N cycles	BR	pre-TMZ	post-TMZ	pre-TMZ	post-TMZ	Lung	Liver	Abdomen	other	Lymph nodes
AR02071	67	M	left colon	KRAS G12D	A	0	19	2	PD	42,12	37,13	2,07	2,68	x			colon	abdominal
AR01032	28	M	rectum	KRAS G13D	A	0	22	1	PD	18,18	26,79	26,55	39,07	x		x		thoracic; abdominal
AR04062	58	F	left colon	KRAS A146T	A	0	25	2	PD	tbd	tbd	tbd	tbd	x	x (❖)	x		
AR01033	65	M	left colon	KRAS T50I	A	0	30	2	PD	29,69	26,79	39,16	39,88	x (2)	x (1)	x		(thoracic; abdominal)
AR01014	46	F	rectum	KRAS G12D	B1	0,31	14	2	PD	17,24	45,01	23,74	55,04	x	x (❖)	x	bone	abdominal
AR01069	51	M	left colon	KRAS G13D/K117N	B1	0,39	26	4	SD	6,73	10,53	0,39	3,18		x	x	bone	
AR03047	53	M	right colon	NRAS Q61K	B1	0,53	36	4	SD	12,44	19,14	5,35	11,33	x	x (❖)			
AR01001	58	F	left colon	KRAS G13D	B1	0,27	38	1	PD	49,76	46,92	52,96	57,81	x	x (3)			
AR01002	49	M	left colon	KRAS G12V	B1	0,3	45	4	SD	12,44	82,37	18,11	18,13	x	(2)	x		thoracic
AR02040	67	F	rectum	KRAS G12V	B1	0,72	61	2	PD	21,05	60,29	44,83	52,88	x	x	x		
AR01041	46	F	right colon	KRAS A59E	B1	0,77	101	2	PD	26,81	62,24	54,57	59,24		x (❖)	x		abdominal
AR02005	67	F	right colon	KRAS G12D	B1	0,72	106	6	SD	NA	188,97	NA	32,86		x	x		
AR01013	69	M	rectum	KRAS G12D	B1	0,63	113	4	SD	20,11	15,31	31,33	19,37	x	x (1)			abdominal; cervical (1)
AR01034	82	M	right colon	KRAS G12S	B1	0,84	137	5	SD	12,69	14,25	1,47	2,01	x	x			
AR02064	62	M	right colon	KRAS G12D	B1	0,77	145	5	SD	4,78	95,26	1,88	4,58	x	x	x		
AR01063	68	F	right colon	KRAS G12D	B1	0,87	176	6	SD	24,88	67,03	27,1	35,19		x		spleen	
AR01015	50	F	left colon	KRAS G13D	B1	0,84	210	6	SD	21,05	19,14	5,74	3,62	x				
AR02011	74	M	left colon	KRAS G12D	B1	0,23	249	6	SD	17,88	18,68	1,41	2,68	x				
AR03049	63	M	left colon	KRAS G12D	B1	0,86	324	4	SD	8,61	NA	10,36	NA	x	x			
AR02007	84	F	left colon	KRAS G12V	B2	0,85	381	6+2	SD	25,84	2276,55	7,25	19,1	x	x (❖)			
AR01052	56	F	left colon	KRAS G12S	B2	0,84	423	6	SD	17,24	195,63	24,89	30,14	x (2)	x (2)		bone	thoracic

Supplementary Table S2:

For each patient, Signature stratification, bTMB, signature score of post TMZ biopsy, best clinical response to TMZ treatment with corresponding genetic localization of the metastases are reported. Patients with preferentially lung localization of the metastases and low shedding of ctDNA in the blood are highlighted in red. *M= male; F= Female; PD = patient with progression disease as best clinical response. SD= patient with stable disease as best clinical response; preTMZ= analysis of tumor before TMZ priming; Post-TMZ= analysis of tumor after TMZ priming; ❖ = Multiple nodules;*

bTMB = blood Tumor Mutational Burden; VAF = Variant Allelic Frequency

Genetic TMZ effect	Patient_ID	TMZ_Signature (score)	MSH6 alterations (post TMZ) in tissue	MSH6 alterations (pre TMZ) in blood	MSH6 alterations (post TMZ) in blood
SUBTYPE A: no genetic TMZ effect	**AR02071**	**0**	-	-	-
SUBTYPE A: no genetic TMZ effect	**AR01032**	**0**	-	-	-
SUBTYPE A: no genetic TMZ effect	**AR04062**	**0**	-	-	-
SUBTYPE A: no genetic TMZ effect	**AR01033**	**0**	-	-	-
SUBTYPE B1: subclonal effect	**AR01014**	**0.31**	-	-	p.T1219I
SUBTYPE B1: subclonal effect	**AR01069**	**0.39**	p.K301fs*12	-	-
SUBTYPE B1: subclonal effect	**AR03047**	**0.53**	-	-	p.T1219I[1]
SUBTYPE B1: subclonal effect	**AR01001**	**0.27**	-	-	p.T1219I
SUBTYPE B1: subclonal effect	**AR01002**	**0.30**	-	-	p.T1219I
SUBTYPE B1: subclonal effect	**AR02040**	**0.72**	-	-	p.T1219I
SUBTYPE B1: subclonal effect	**AR01041**	**0.77**	-	-	p.T1219I
SUBTYPE B1: subclonal effect	**AR02005**	**0.72**	p.T1219I;p.G557D	NA	p.T1219I;p.G557D; p.Q626*; p.W456*; p.W413*; p.G520D; p.G1157D; p.T1008I
SUBTYPE B1: subclonal effect	**AR01013**	**0.63**	-	-	p.T1219I
SUBTYPE B1: subclonal effect	**AR01034**	**0.84**	p.T1219I;p.G557D; p.V777*; p.W50*	-	p.T1219I
SUBTYPE B1: subclonal effect	**AR02064**	**0.77**	-	-	Q1122*; p.T1219I
SUBTYPE B1: subclonal effect	**AR01063**	**0.87**	p.W1047*	-	p.T1219I;p.S1188N; p.Q485*
SUBTYPE B1: subclonal effect	**AR01015**	**0.84**	p.T1219I	-	p.T1219I
SUBTYPE B1: subclonal effect	**AR02011**	**0.23**	p.T1219I	-	p.T1219I
SUBTYPE B1: subclonal effect	**AR03049**	**0.86**	p.T1219I	-	NA
SUBTYPE B2: clonal effect	**AR02007**	**0.85**	p.G1139S	-	p.G1139S; p.T1219I; p.Q1122*; p.W142*; p.Q1314*; p.W372*; p.Q244*
SUBTYPE B2: clonal effect	**AR01052**	**0.84**	-	-	p.T1219I;p.T1008I

Fig. 1

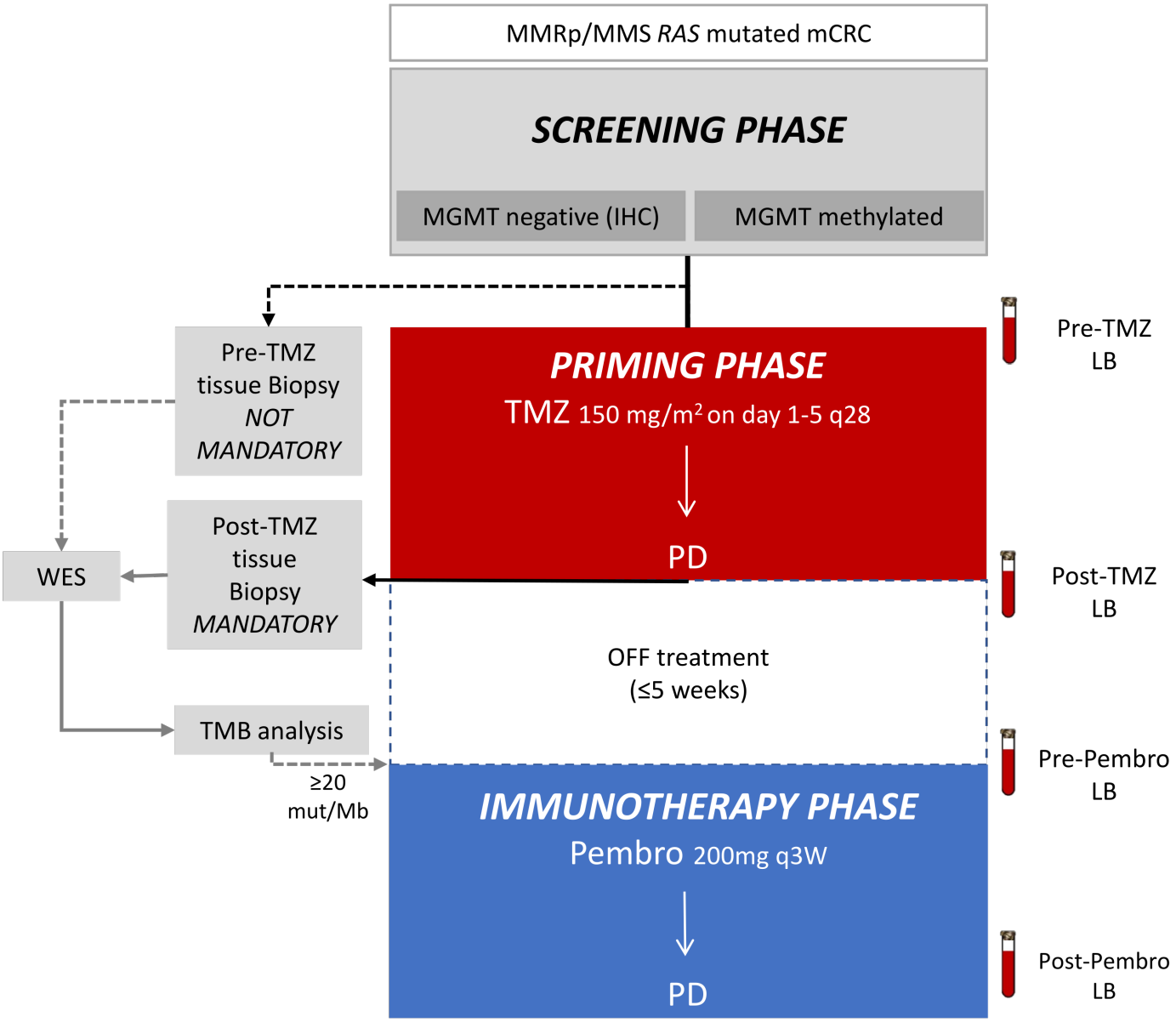
MMRp/MMS *RAS* mutated mCRC
SCREENING PHASE
MGMT negative (IHC)
MGMT methylated
Pre-TMZ tissue Biopsy *NOT MANDATORY*
PRIMING PHASE
TMZ 150 mg/m² on day 1-5 q28
PD
Pre-TMZ LB
Post-TMZ tissue Biopsy *MANDATORY*
WES
Post-TMZ LB
OFF treatment (≤5 weeks)
TMB analysis
≥20 mut/Mb
Pre-Pembro LB
IMMUNOTHERAPY PHASE
Pembro 200mg q3W
PD
Post-Pembro LB

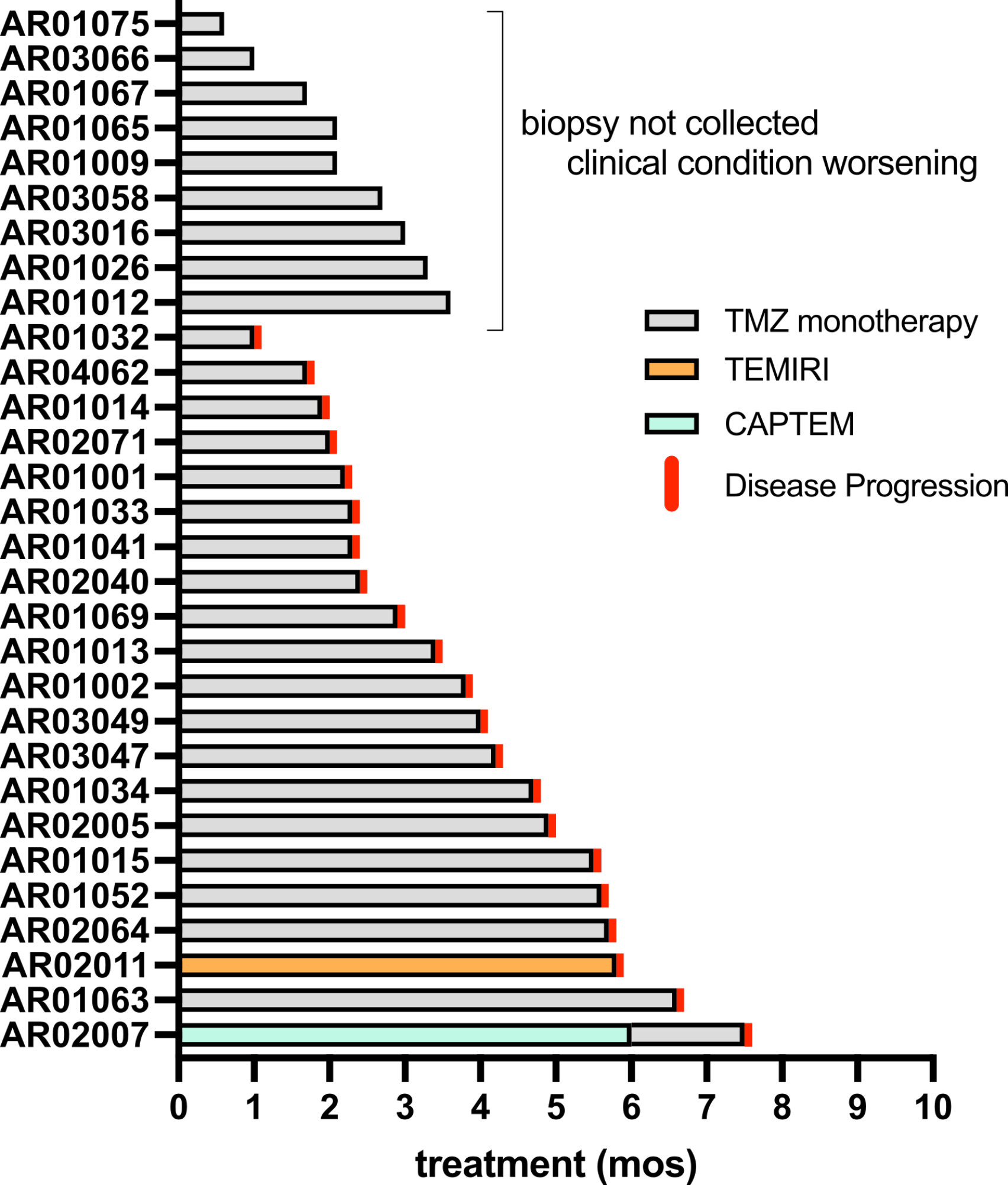
AR01075
AR03066
AR01067
AR01065
AR01009
AR03058
AR03016
AR01026
AR01012
AR01032
AR04062
AR01014
AR02071
AR01001
AR01033
AR01041
AR02040
AR01069
AR01013
AR01002
AR03049
AR03047
AR01034
AR02005
AR01015
AR01052
AR02064
AR02011
AR01063
AR02007
biopsy not collected
clinical condition worsening
TMZ monotherapy
TEMIRI
CAPTEM
Disease Progression
0
1
2
3
4
5
6
7
8
9
10
treatment (mos)

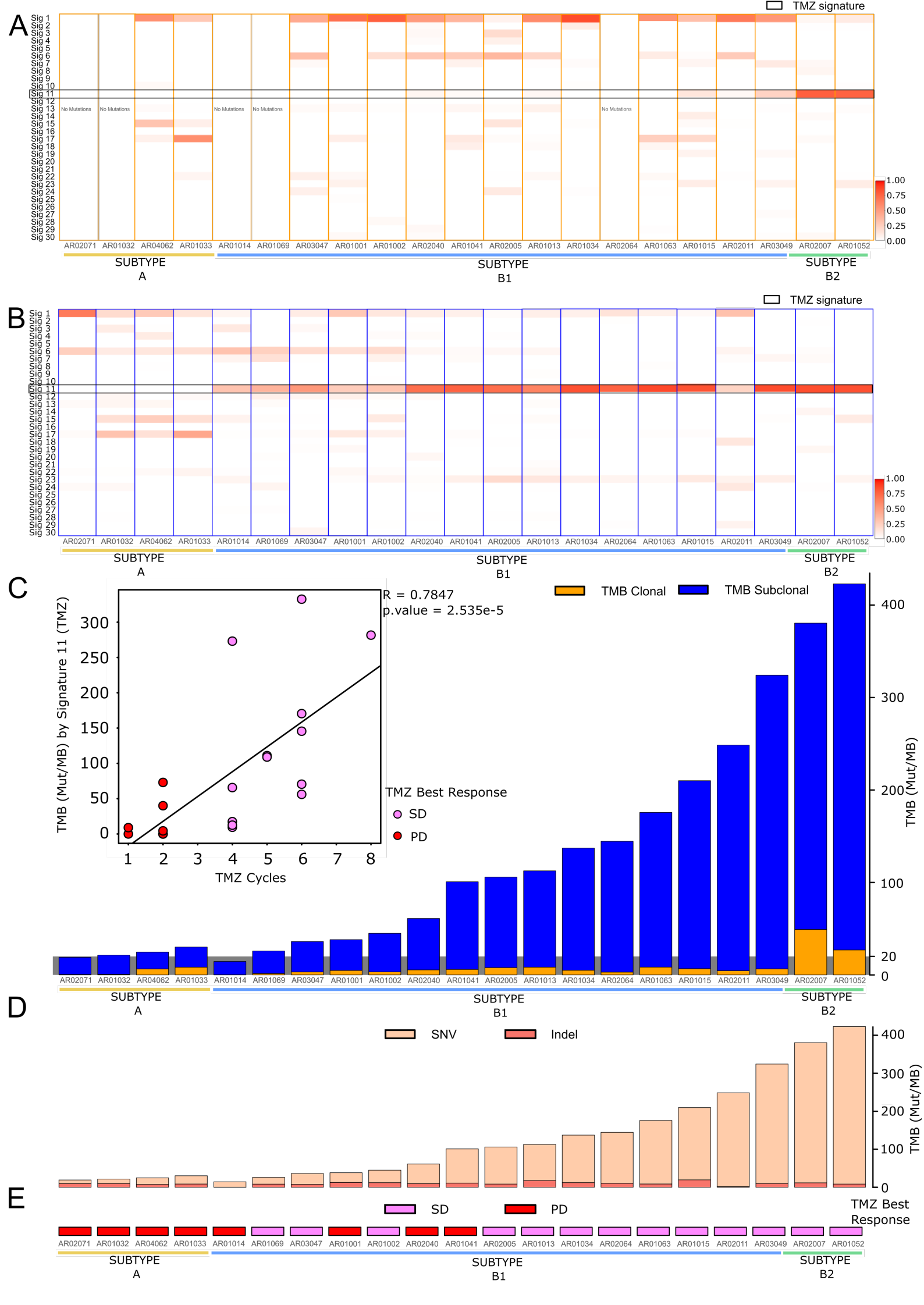
A
TMZ signature
Sig 1
Sig 2
Sig 3
Sig 4
Sig 5
Sig 6
Sig 7
Sig 8
Sig 9
Sig 10
Sig 11
Sig 12
Sig 13
Sig 14
Sig 15
Sig 16
Sig 17
Sig 18
Sig 19
Sig 20
Sig 21
Sig 22
Sig 23
Sig 24
Sig 25
Sig 26
Sig 27
Sig 28
Sig 29
Sig 30
No Mutations
1.00
0.75
0.50
0.25
0.00
AR02071 AR01032 AR04062 AR01033 AR01014 AR01069 AR03047 AR01001 AR01002 AR02040 AR01041 AR02005 AR01013 AR01034 AR02064 AR01063 AR01015 AR02011 AR03049 AR02007 AR01052
SUBTYPE A
SUBTYPE B1
SUBTYPE B2
B
TMZ signature
C
TMB (Mut/MB) by Signature 11 (TMZ)
R = 0.7847
p.value = 2.535e-5
TMZ Best Response
SD
PD
TMZ Cycles
TMB Clonal
TMB Subclonal
TMB (Mut/MB)
D
SNV
Indel
E
SD
PD
TMZ Best Response

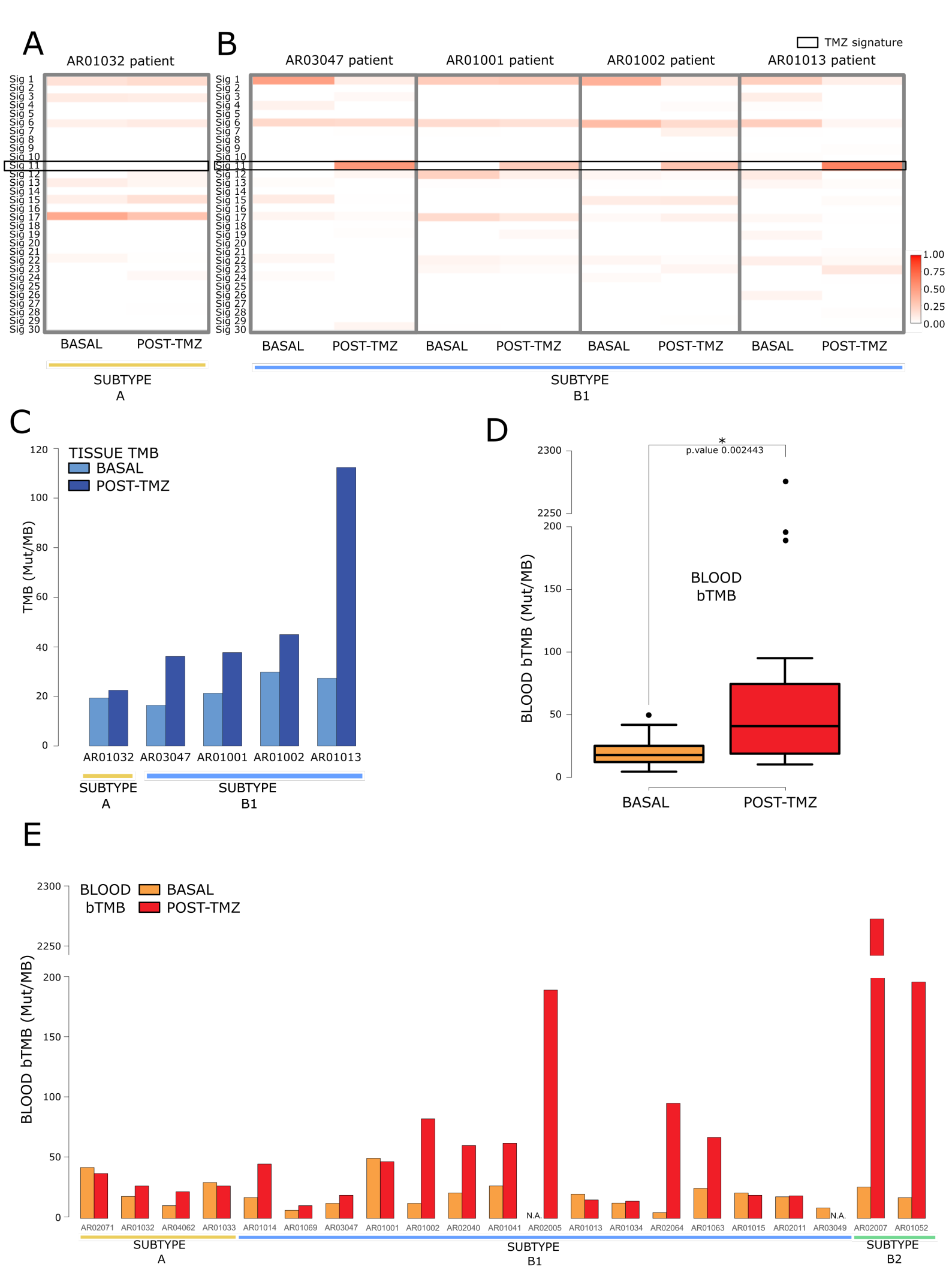
A
AR01032 patient
B
AR03047 patient
AR01001 patient
AR01002 patient
AR01013 patient
TMZ signature
Sig 1
Sig 2
Sig 3
Sig 4
Sig 5
Sig 6
Sig 7
Sig 8
Sig 9
Sig 10
Sig 11
Sig 12
Sig 13
Sig 14
Sig 15
Sig 16
Sig 17
Sig 18
Sig 19
Sig 20
Sig 21
Sig 22
Sig 23
Sig 24
Sig 25
Sig 26
Sig 27
Sig 28
Sig 29
Sig 30
1.00
0.75
0.50
0.25
0.00
BASAL
POST-TMZ
SUBTYPE A
SUBTYPE B1
C
TISSUE TMB
BASAL
POST-TMZ
TMB (Mut/MB)
AR01032
AR03047
AR01001
AR01002
AR01013
SUBTYPE A
SUBTYPE B1
D
p.value 0.002443
BLOOD bTMB
BLOOD bTMB (Mut/MB)
BASAL
POST-TMZ
E
BLOOD bTMB
BASAL
POST-TMZ
BLOOD bTMB (Mut/MB)
AR02071
AR01032
AR04062
AR01033
AR01014
AR01069
AR03047
AR01001
AR01002
AR02040
AR01041
AR02005
AR01013
AR01034
AR02064
AR01063
AR01015
AR02011
AR03049
AR02007
AR01052
N.A.
SUBTYPE A
SUBTYPE B1
SUBTYPE B2

A

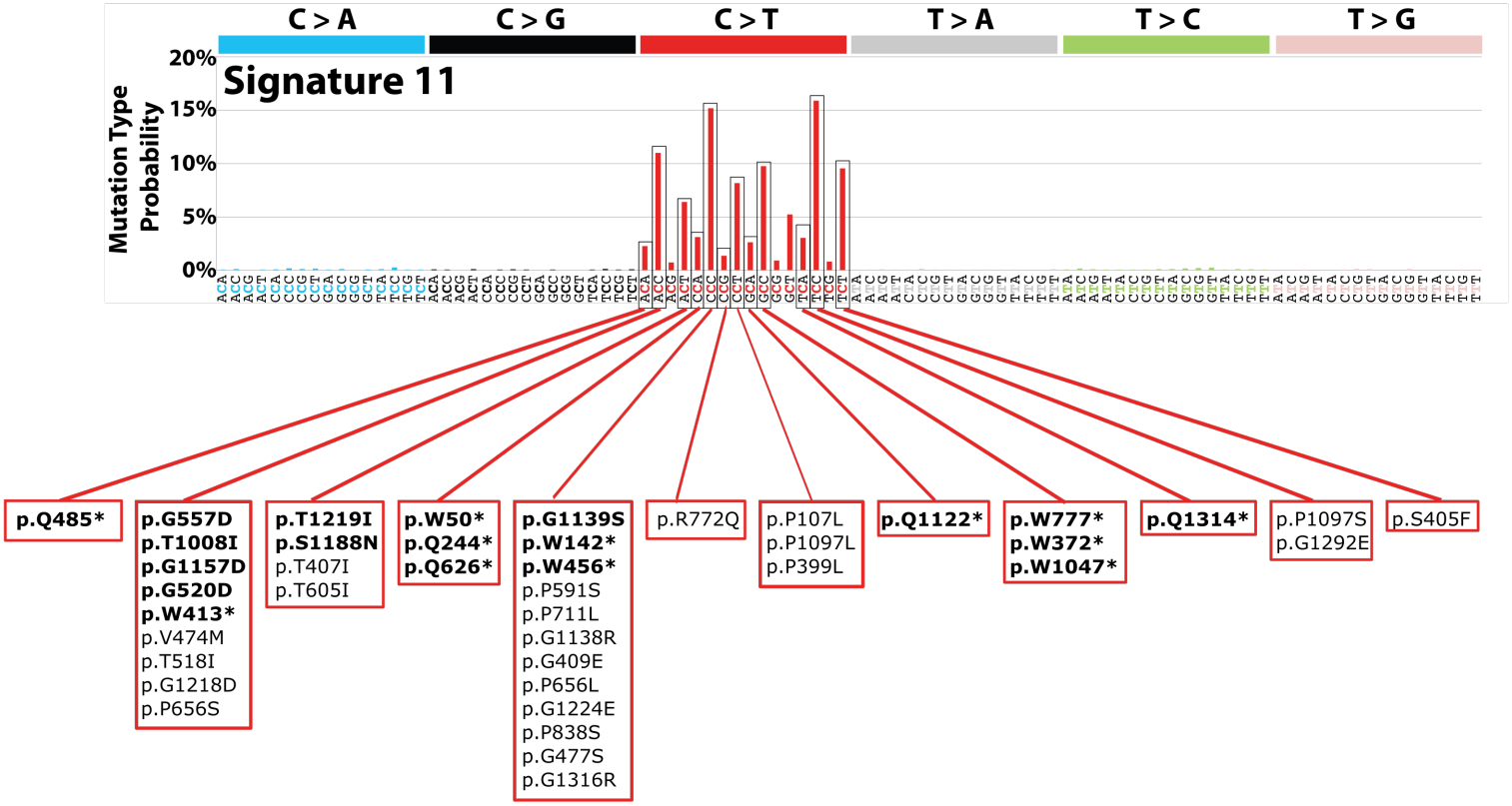

B

MSH6 alteration	coord	Patient	Patient_ID	dMMR status
p.T1219I	chr2:48033352	16	AR01014; AR01001; AR01002; AR02005; AR010013; AR01015; AR01034; AR01041; AR02040; AR02011; AR02007; AR03049; AR01052; AR01063;AR02064; AR03047	Drost et al., 2020
p.G557D	chr2:48026792	2	AR01034; AR02005	Drost et al., 2020
p.T1008I	chr2:48028145	2	AR02005; AR01052	Drost et al., 2020
p.Q1122*	chr2:48030750	2	AR02007; AR02064	STOP codon acquisition
p.W777*	chr2:48027453	1	AR01034	STOP codon acquisition
p.W50*	chr2:48010521	1	AR01034	STOP codon acquisition
p.G1139S	chr2:48030801	1	AR02007	Drost et al., 2020
p.W142*	chr2:48018231	1	AR02007	STOP codon acquisition
p.Q1314*	chr2:48033729	1	AR02007	STOP codon acquisition
p.W372*	chr2:48026238	1	AR02007	STOP codon acquisition
p.Q244*	chr2:48025852	1	AR02007	STOP codon acquisition
p.G1157D	chr2:48032080	1	AR02005	Drost et al., 2020
p.G520D	chr2:48026681	1	AR02005	Drost et al., 2020
p.W413*	chr2:48026361	1	AR02005	STOP codon acquisition
p.W456*	chr2:48026490	1	AR02005	STOP codon acquisition
p.Q626*	chr2:48026998	1	AR02005	STOP codon acquisition
p.W1047*	chr2:48028263	1	AR01063	STOP codon acquisition
p.S1188N	chr2:48032763	1	AR01063	Drost et al., 2020
p.Q485*	chr2:48026575	1	AR01063	STOP codon acquisition
p.K301fs*12	chr2:48026024	1	AR01069	STOP codon acquisition
p.G409E	chr2:48026348	2	AR02040; AR01063	
p.P591S	chr2:48026893	1	AR02005	
p.P107L	chr2:48018125	1	AR02005	
p.P711L	chr2:48027254	1	AR02005	
p.P1097S	chr2:48030675	1	AR02005	
p.V474M	chr2:48026542	1	AR01013	
p.P1097L	chr2:48030676	1	AR01015	
p.G1292E	chr2:48033664	1	AR01015	
p.R772Q	chr2:48027437	1	AR01015	
p.G1138R	chr2:48030798	1	AR01034	
p.S405F	chr2:48026336	1	AR02040	
p.P656L	chr2:48027089	1	AR02011	
p.P656S	chr2:48027088	1	AR02064	
p.P399L	chr2:48026318	1	AR02064	
p.P838S	chr2:48027634	1	AR01063	
p.T518I	chr2:48026675	1	AR01063	
p.G477S	chr2:48026551	1	AR01063	
p.G1218D	chr2:48033349	1	AR01063	
p.G1316R	chr2:48033735	1	AR01063	
p.T407I	chr2:48026342	1	AR02007	
p.G1224E	chr2:48033367	1	AR02007	
p.T605I	chr2:48026936	1	AR02007	

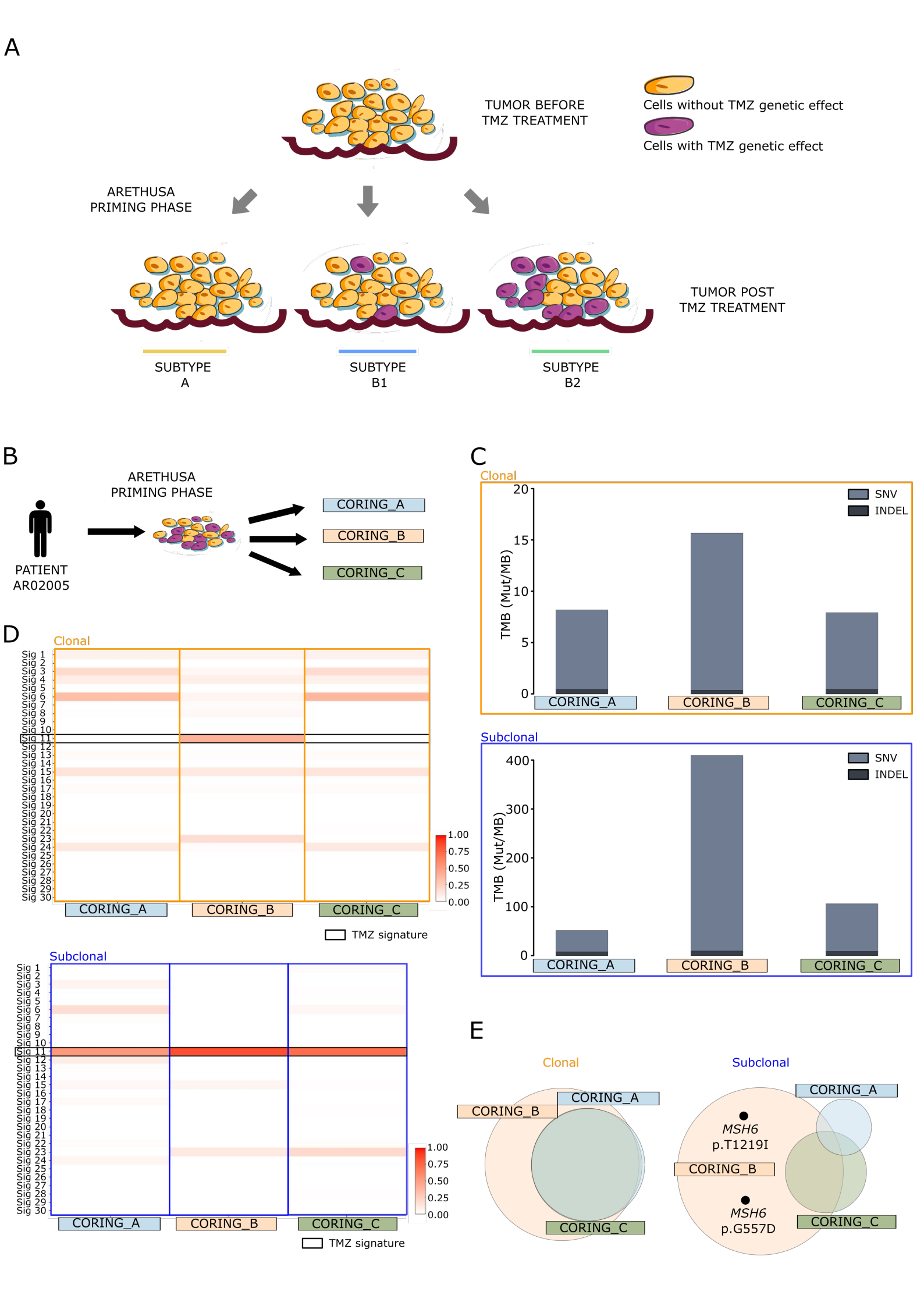
A
TUMOR BEFORE
TMZ TREATMENT
Cells without TMZ genetic effect
Cells with TMZ genetic effect
ARETHUSA
PRIMING PHASE
TUMOR POST
TMZ TREATMENT
SUBTYPE
A
SUBTYPE
B1
SUBTYPE
B2
B
ARETHUSA
PRIMING PHASE
PATIENT
AR02005
CORING_A
CORING_B
CORING_C
C
Clonal
SNV
INDEL
TMB (Mut/MB)
0
5
10
15
20
CORING_A
CORING_B
CORING_C
Subclonal
SNV
INDEL
TMB (Mut/MB)
0
100
200
300
400
CORING_A
CORING_B
CORING_C
D
Clonal
Sig 1
Sig 2
Sig 3
Sig 4
Sig 5
Sig 6
Sig 7
Sig 8
Sig 9
Sig 10
Sig 11
Sig 12
Sig 13
Sig 14
Sig 15
Sig 16
Sig 17
Sig 18
Sig 19
Sig 20
Sig 21
Sig 22
Sig 23
Sig 24
Sig 25
Sig 26
Sig 27
Sig 28
Sig 29
Sig 30
CORING_A
CORING_B
CORING_C
1.00
0.75
0.50
0.25
0.00
TMZ signature
Subclonal
Sig 1
Sig 2
Sig 3
Sig 4
Sig 5
Sig 6
Sig 7
Sig 8
Sig 9
Sig 10
Sig 11
Sig 12
Sig 13
Sig 14
Sig 15
Sig 16
Sig 17
Sig 18
Sig 19
Sig 20
Sig 21
Sig 22
Sig 23
Sig 24
Sig 25
Sig 26
Sig 27
Sig 28
Sig 29
Sig 30
CORING_A
CORING_B
CORING_C
1.00
0.75
0.50
0.25
0.00
TMZ signature
E
Clonal
CORING_A
CORING_B
CORING_C
Subclonal
CORING_A
MSH6
p.T1219I
CORING_B
MSH6
p.G557D
CORING_C

Fig 7

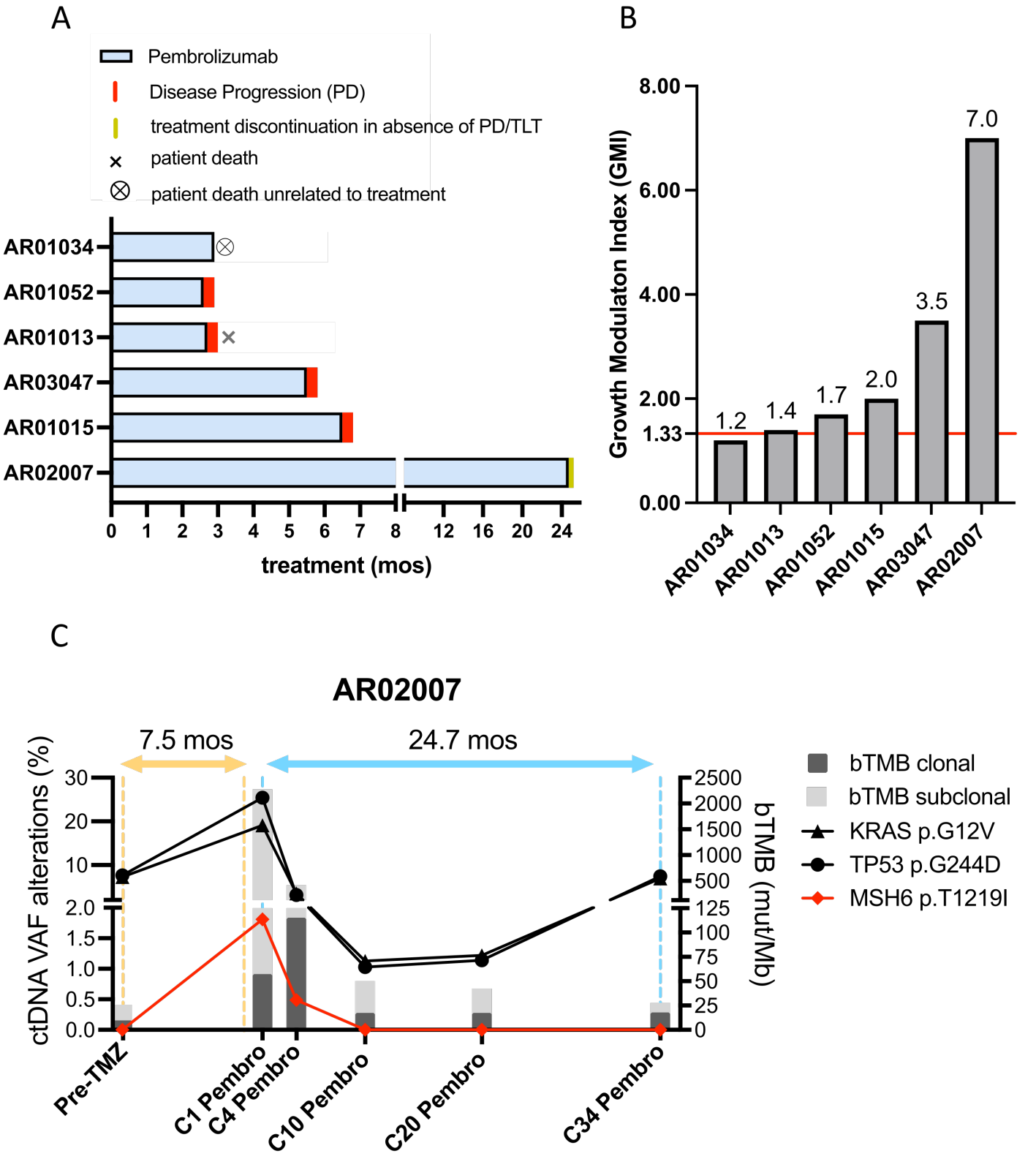
A
Pembrolizumab
Disease Progression (PD)
treatment discontinuation in absence of PD/TLT
patient death
patient death unrelated to treatment
AR01034
AR01052
AR01013
AR03047
AR01015
AR02007
0 1 2 3 4 5 6 7 8 12 16 20 24
treatment (mos)
B
Growth Modulaton Index (GMI)
8.00
6.00
4.00
2.00
1.33
0.00
1.2
1.4
1.7
2.0
3.5
7.0
AR01034
AR01013
AR01052
AR01015
AR03047
AR02007
C
AR02007
7.5 mos
24.7 mos
ctDNA VAF alterations (%)
30
20
10
2.0
1.5
1.0
0.5
0.0
2500
2000
1500
1000
500
125
100
75
50
25
0
bTMB (mut/Mb)
bTMB clonal
bTMB subclonal
KRAS p.G12V
TP53 p.G244D
MSH6 p.T1219I
Pre-TMZ
C1 Pembro
C4 Pembro
C10 Pembro
C20 Pembro
C34 Pembro